Single-shot Quantum Signal Processing Interferometry

Jasmine Sinanan-Singh,[1, *] Gabriel L. Mintzer,[2, 3, *] Isaac L. Chuang,[1, 3] and Yuan Liu [1, †]

[1] *Department of Physics, Co-Design Center for Quantum Advantage,*
Massachusetts Institute of Technology, Cambridge, Massachusetts 02139, USA
[2] *Department of Physics, Massachusetts Institute of Technology, Cambridge, Massachusetts 02139, USA*
[3] *Department of Electrical Engineering and Computer Science,*
Massachusetts Institute of Technology, Cambridge, Massachusetts 02139, USA
(Dated: November 27, 2023)

Quantum systems of infinite dimension, such as bosonic oscillators, provide vast resources for quantum sensing. Yet, a general theory on how to manipulate such bosonic modes for sensing beyond parameter estimation is unknown. We present a general algorithmic framework, quantum signal processing interferometry (QSPI), for quantum sensing at the fundamental limits of quantum mechanics, i.e., the Heisenberg sensing limit, by generalizing Ramsey-type interferometry. Our QSPI sensing protocol relies on performing nonlinear polynomial transformations on the oscillator's quadrature operators by generalizing quantum signal processing (QSP) from qubits to hybrid qubit-oscillator systems. We use our QSPI sensing framework to make binary decisions on a displacement channel in the single-shot limit. Theoretical analysis suggests the sensing accuracy given a single-shot qubit measurement can approach the Heisenberg-limit scaling. We further concatenate a series of such binary decisions to perform parameter estimation in a bit-by-bit fashion. Numerical simulations are performed to support these statements. Our QSPI protocol offers a unified framework for quantum sensing using continuous-variable bosonic systems beyond parameter estimation and establishes a promising avenue toward efficient and scalable quantum control and quantum sensing schemes beyond the NISQ era.

CONTENTS

* These two authors contributed equally.
† yuanliu@mit.edu

I. INTRODUCTION

Sensing and metrology are fundamental pursuits of science and technology, and quantum systems have been used to advance metrological precision to new bounds [1–4]. Typical quantum sensing protocols involve manipulation of quantum coherence and entanglement followed by measurement to extract useful classical information from quantum systems.

The efficiency of different quantum sensing protocols varies by construction. At a high level, any sensing protocol can be assessed by the space and time resource requirements (e.g., the size of the quantum sensor, any required repetition of the experiments, the length of the sensing protocol) it needs to achieve a given sensitivity in the sensing task, for example estimating a given parameter to a certain precision. The intrinsic probabilistic nature of quantum systems necessarily introduces uncertainty to the measurement of any sensing protocol, leading to the so-called standard quantum limit (SQL). In the SQL, the standard deviation of the estimated parameter scales inversely as the square-root of the space and time resources employed, as is familiar in processes involving shot noise.

By leveraging non-classical properties of quantum states like entanglement [5, 6] and general quantum correlations [7] as resources for sensing, sensitivity in parameter estimation can be improved beyond the SQL to approach a more fundamental physical limit, the Heisenberg limit (HL). The HL dictates that the scaling of precision with total sensing time t can be no better than $1/t$; equivalently, with N probes used in an experiment, the precision scales no better than $1/N$.

In fact, this fundamental physical limit has been achieved by a number of sensing protocols. One of the oldest and best-known is the interferometric protocol known as cat-state sensing, named after Schrödinger's cat for its use of superpositions of two distinct macroscopic states, such as the all-spin-up and all-spin-down states in a multi-atom system. This protocol, first realized for spin-states in 1996 by Bollinger et al., achieves the optimal bound for frequency uncertainty of an N-particle system [8]. This optimal HL bound, equal to $(NT)^{-1}$, where T is the time for a single repetition of the protocol, is achieved by modifying the Ramsey technique [9] to use a maximally correlated GHZ state and a different final measurement operator. As it achieves the HL limit, this variety of cat-state sensing for spin systems has found broad application in precision phase sensing for atomic clocks [10, 11], where variational quantum algorithms are incorporated into multi-qubit Ramsey interferometry to iteratively optimize the sensing precision.

However, many other parameters of interest, such as electric fields [12], can be better sensed by bosonic modes (e.g., photonic and phononic oscillators) than spin systems. Bosonic sensors have been employed to perform precision sensing of small displacements to bosonic oscillators, and there have been many advances investigating the advantages of utilizing bosonic resource states [13, 14]. Gilmore et al. have found that coupling the spins of a trapped-ion crystal to their collective motional mode offers sub-SQL sensing performance, with the quantum enhancement achieved through interferometry of highly-entangled spin-motion cat states [15]. Using the interference between squeezed light, the Advanced LIGO [16] experiment can detect the space-time curvature change caused by gravitational

waves. Additionally, coupling bosonic modes to other degrees of freedom can transfer information from one subsystem to another in order to facilitate more convenient measurement than the direct measurement of the bosonic modes themselves [17]. In spectroscopy, entangled cat-state laser sources have also been used to enhance signals by an order of magnitude [18]. Beyond the single-mode case, it has been demonstrated that the entanglement of many modes can provide HL-sensing enhancement [19, 20]. Furthermore, various efficient HL-scaling Hamiltonian learning protocols have been proposed, including some on bosonic systems, that can be rephrased as multi-parameter estimation problems [21, 22].

Beyond parameter estimation, there are many other sensing applications that have been left largely unexplored, for example, single-shot decision making. For such decision-making problems, the underlying signal can happen rarely, such as the case of gravitational wave detection [1], and it is therefore crucial to obtain useful information in the single-shot limit. When events are rare, many iterative protocols for parameter estimation and learning [22, 23] are challenged. Despite the success of bosonic systems and cat state sensing for parameter estimation, a unified protocol for general sensing tasks is unknown, particularly in scenarios where decisions must be made in the single-shot limit.

Protocols for realizing such general sensing tasks should generally build on the ability to perform transformations of the underlying signal. Not surprisingly, transformation of classical signals has been extensively studied in the context of *signal processing* in electrical engineering [24], where state-of-the-art classical algorithms have been developed to design a variety of *filters* that transform the underlying classical signals tailored to the desired purposes [25, 26]. Inspired by classical signal processing, quantum signal processing (QSP) algorithms [27–39] can achieve arbitrary polynomial transformations on one or more quantum amplitudes. Given the triumphs of classical and quantum signal processing, might it be possible to adopt the philosophy of filter design to bosonic systems such that quantum signals on oscillators can be transformed for general sensing tasks?

In the present work, we develop a novel algorithmic protocol for general quantum sensing tasks beyond parameter estimation using interferometric bosonic modes in a way which enables systematic and analytically predictive improvement of single-shot decision error beyond what is possible with traditional sensing protocols. This *QSP interferometry (QSPI)* protocol builds on a theory of bosonic QSP that can perform polynomial transformation on the block-encoded quadrature operators of bosonic modes using qubit rotations and qubit-oscillator entangling gates [40, 41]. The core of our QSPI protocol lies in these polynomial transformations generating nonclassical resource states for interferometery. Just as in typical Ramsey

experiments [9], the signal being sensed in a QSPI experiment is queried only once, and the power of quantum enhancement comes from generating a non-classical resource state by increasing the QSP circuit length. This single-shot feature distinguishes our work from much prior art [21–23].

We demonstrate the performance of the QSPI protocol with a theoretical analysis which optimally extracts binary decision information about a quantum displacement channel, achieving HL-like scaling (see Def. 1). As a concrete pedagogical example, we focus on the task of distinguishing whether a displacement channel has a displacement amount above or below a given threshold. Note that such decision problems are ideal for qubit-oscillator systems because we desire a single-shot measurement that answers a question about the channel acting on a bosonic quantum state with high probability. Given that the qubit is naturally binary under classical projection measurement, extracting a yes/no answer from the qubit should be much faster than extracting a continuous-valued answer by measuring the oscillator. This intuition is satisfied by our construction. We also show how to utilize protocols for such simple decision problems to perform more complex tasks such as bit-by-bit estimation of the magnitude of a displacement.

The presentation below is organized as follows. We begin in Sec. II with a formal statement of the problem scenario and the expected performance using traditional cat-state sensing, then build on this to exhibit the new quantum signal processing interferometry protocol and its provably improved performance in Sec. III. Building upon this, Sec. IV analyzes analytically the performance of our QSPI protocol for making binary decisions about the displacement parameter. Sec. V then demonstrates the use of such a decision-making subroutine to perform parameter estimation on the magnitude of a displacement by combining with classical decision-making theory. Sec. VI presents numerical results, revealing a Heisenberg-limit-like scaling in the decision error, agreeing with analytical expectations. Conclusions and outlook are given in Sec. VII.

II. A BINARY BOSONIC DECISION PROBLEM

In this section, we first set up some notation and define quantum decision-making problem in displacement sensing, as well as what HL-like behavior is for decision problems in Sec. II A. In Sec. II B we review the basics of a typical displacement-sensing protocol based on cat-state interferometry, highlighting its advantages and limitations to motivate why a more general sensing scheme is required.

A. Quantum Decision-Making for a Displacement Channel

We consider a quantum sensing problem in a joint qubit-oscillator system subjected to a unitary displacement channel S_β

$$S_\beta := \begin{bmatrix} e^{i\beta\hat{p}} & 0 \\ 0 & e^{i\beta\hat{p}} \end{bmatrix}, \qquad (1)$$

where we have written S_β under the joint qubit-oscillator tensor product form such that $S_\beta = I \otimes e^{i\beta\hat{p}}$ and β is the amount of the position kick acting on the oscillator; $e^{i\beta\hat{p}}|x\rangle_{\text{osc}} = |x - \beta\rangle_{\text{osc}}$ for a position eigenstate $|x\rangle_{\text{osc}}$ (the subscript "osc" refers to "oscillator" to distinguish it from the qubit register). The symbol := represents definition of a quantity, and $\hat{x}$, $\hat{p}$ are the oscillator's canonical position and momentum operators, respectively. On the joint system, we assume the resource gates are arbitrary single-qubit rotations $R_X(2\theta) := e^{i\theta\sigma_x}$ and a fixed qubit-oscillator entangling gate

$$\mathcal{D}_c(i\kappa/\sqrt{2}) = e^{i\kappa\hat{x}\sigma_z} \qquad (2)$$

parameterized by κ, where $\mathcal{D}_c(i\kappa/\sqrt{2})$ is a conditional displacement gate that imparts a momentum kick $\pm\kappa$ to the oscillator depending on the qubit state being $|0\rangle$ or $|1\rangle$. σ_x, σ_z are the single-qubit Pauli matrices. This entangling gate is derived from the usual definition of a more general conditional displacement gate in phase space $\mathcal{D}_c(\alpha) := e^{(\alpha a^\dagger - \alpha^* a)\sigma_z}$ by setting $\alpha = i\kappa/\sqrt{2}$. Moreover, the gate in Eq. (2) is an operator with support on the infinite-dimensional qubit-oscillator joint Hilbert space. When acting on a position eigenstate of the oscillator $|x\rangle_{\text{osc}}$, the gate given in Eq. (2) reduces to $e^{i\kappa x\sigma_z}$ which is simply a 2×2 operator acting on the qubit. Throughout the paper, we shall use $\hat{x}$, $\hat{p}$ and x, p to distinguish the two different ways of using position and momentum as operators or real numbers. The product of $\kappa\hat{x}$ on the right-hand side of Eq. (2) also means the gate itself will be periodic in the oscillator position x with a period of $T_x = \frac{2\pi}{\kappa}$.

With these notations established, we are ready to define the quantum decision-making problem on the displacement channel:

Main Problem (Quantum Binary Decision-Making for a Displacement Channel). *Given $\beta_{\text{th}} > 0$, construct a quantum circuit by using the resource gates R_X and $\mathcal{D}_c(i\kappa/\sqrt{2})$ a maximum of d times for some κ to determine whether $|\beta| > \beta_{\text{th}}$ or $|\beta| < \beta_{\text{th}}$ with only a single query to S_β, such that the probability of making an erroneous decision, p_{err}, is small.*

Clearly, the probability p_{err} of erroneous decision will depend on $\kappa, \beta_{\text{th}}$, and d. Due to the periodicity of Eq. (2) in x, any unitary constructed from repeated applications of $\mathcal{D}_c(i\kappa/\sqrt{2})$ and R_X will be periodic in x with the same period T_x. As will be discussed in Sec. III C (also see

Fig. 3), the periodicity in x for the $\mathcal{D}_c(\cdot)$ gate results in a period of $T_x/2$ for p_{err} in terms of the sensing parameter β. This allows us to define a restricted region $(-\frac{\pi}{2\kappa}, \frac{\pi}{2\kappa})$ where the sensing problem will be discussed. This notion of periodicity is similar to the concept of a "unit cell" in solid state physics [42]. Therefore, it is necessary to choose κ to be small enough such that $\beta \in (-\frac{\pi}{2\kappa}, \frac{\pi}{2\kappa})$ (in particular, β_{th} as well). However, κ cannot be too small, or else $\mathcal{D}_c(i\kappa/\sqrt{2})$ will become too close to the identity operator, and its action on the qubit-oscillator system will not be effective. In the rest of the paper, we assume that κ has been fixed with these conditions satisfied. Furthermore, (as detailed in Appendix B) p_{err} is an even function of β; therefore, we only consider the case of $\beta_{\text{th}} > 0$, as given in Main Problem.

Once we are given β_{th} and have fixed κ as described above, it is instructive to consider how p_{err} scales as the number of resource gates d in the sensing protocol. In the single-shot limit, since we are only allowed to query the signal S_β once, it is not difficult to see that the most general single-shot decision-making protocol is as given in Fig. 1a, where a state preparation routine is first used to prepare the joint qubit-oscillator system at some entangled quantum state, after which the signal of interest occurs to the oscillator. In the end, a signal decoding operation is applied to create some interference followed by a single-qubit measurement to extract the answer to the decision problem. Inspired by the definition of HL scaling in parameter estimation tasks, as discussed in Sec. I, we define HL-like scaling for the Main Problem:

Definition 1 (HL-like Scaling for Binary Decision error in the Main Problem.). *A sensing protocol achieves Heisenberg-limit-like (HL-like) scaling for binary decision-making with a displacement channel in the Main Problem if the resulting $p_{\text{err}} \sim O(1/d)$ up to a factor of polylog($1/d$).*

In the following section, we will consider a concrete realization of the general single-shot decision-making protocol (Fig. 1a), the cat state sensing protocol, to gain some intuition.

B. Intuition from Cat-State Sensing

The intuition for building a QSP interferometer comes from the cat-state protocol for sensing small displacements. A typical sensing scheme is shown in Fig. 1b where a Hadamard gate and a controlled displacement $\mathcal{D}_c(i\kappa/\sqrt{2}) = e^{i\kappa\hat{x}\sigma_z}$ are first used to prepare an entangled state of the qubit-oscillator joint system from an initial state of qubit at $|\downarrow\rangle$ and oscillator at vacuum $|0\rangle_{\text{osc}}$ (first dashed blue box). The subscript c in $\mathcal{D}_c(\cdot)$ means the displacement is controlled by the qubit. Then the underlying signal (a displacement $S_\beta = e^{i\beta\hat{p}}$) is applied to the oscillator and followed by another controlled displacement and a Hadamard gate (inverse of

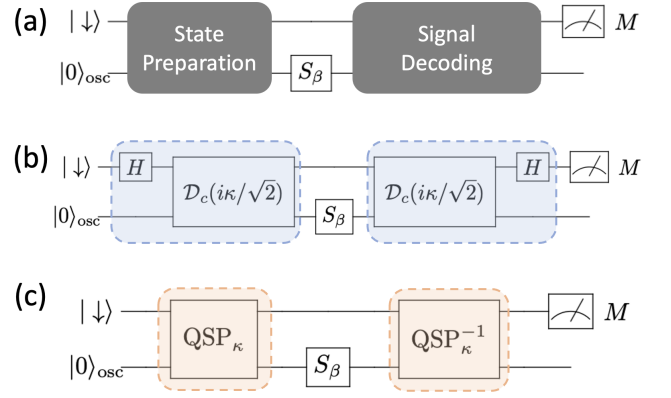the previous dashed blue box). Finally, a qubit Z-basis measurement is performed.

FIG. 1. The most general single-shot decision-making protocol (a), and two realizations comparing the traditional cat-state sensing protocol (b) with the novel bosonic QSP interferometric protocol (c). In (c), the QSP operator creates an optimal sensing state, which then probes the signal S_β and is finally un-created to produce desired interference, which is followed by a measurement on the qubit.

Using the commutation relationship between $\hat{x}$ and $\hat{p}$ we have the following relation

$$e^{i\kappa\hat{x}}e^{i\beta\hat{p}} = e^{i\beta\hat{p}}e^{i\kappa\hat{x}}e^{-i\kappa\beta}, \qquad (3)$$

which simplifies the final state of the joint qubit-oscillator system before the measurement to

$$|\Psi_{\text{out}}\rangle = (\cos(\kappa\beta)\,|\downarrow\rangle + i\sin(\kappa\beta)\,|\uparrow\rangle) \otimes e^{-i\beta\hat{p}}\,|0\rangle_{\text{osc}}, \quad (4)$$

provided that the initial state is $|\downarrow\rangle \otimes |0\rangle_{\text{osc}}$. Therefore, the displacement β is encoded in the amplitude of the ancilla qubit, where the measurement probability p of the qubit in $|\downarrow\rangle$ is

$$p = \text{Prob}[M = \downarrow] = \cos^2(\kappa\beta). \qquad (5)$$

Since κ is known, we can repeat this sensing protocol multiple times in order to obtain an estimate of this probability, which will then tell us the value of β.

More concretely, by repeating the protocol N times, the standard deviation for estimating β is given by $\Delta\beta$:

$$\Delta\beta = \frac{\Delta p}{\left|\frac{dp}{d\beta}\right|} = \frac{1}{2\kappa\sqrt{N}} \qquad (6)$$

where $\Delta p = \sqrt{\frac{p(1-p)}{N}}$ is the standard deviation on p, estimated by performing N experiments with a Bernoulli distribution, and the total time t for repeating the sensing protocol N times will be $t \propto N$. An interesting observation immediately follows from Eq. (6): for fixed N, $\Delta\beta$ improves roughly as $1/\kappa$, where κ is the displacement amount of the $\mathcal{D}_c(\cdot)$ gate. The physical intuition is that the cat state's small interference features

in phase space have a characteristic length of $1/\kappa$. As a result, the sensitivity on estimating a spatial variation in β improves as $1/\kappa$. It follows that taking κ large would be beneficial to making high-sensitivity measurements. Such large κ can be realized in several ways, depending on the physical platform. For example, in trapped ions, a large κ may be realized by increasing the laser pulse intensity or by increasing the pulse duration [40].

Despite its favorable sensing scaling in κ for displacement sensing, the cat-state sensing protocol has some limitations. First, for fixed κ, $\Delta\beta$ decreases as $\frac{1}{\sqrt{N}}$ (or $\frac{1}{\sqrt{t}}$) as the number of classical repetitions N increases. This is the typical shot noise statistical convergence rate corresponding to the SQL and is sub-optimal as compared with HL scaling. Second, aside from parameter estimation on β, the cat-state sensing protocol is not particularly useful if we are only interested in learning partial information about the properties of β, for example determining if β is above or below a given threshold value β_{th}. Since only partial information is needed in such scenarios, it is expected that more efficient sensing protocols exist.

As alluded to earlier in the Introduction, filter designs in classical signal processing and advancement in quantum algorithms provide possibilities for overcoming the two aforementioned limitations such that: 1) Heisenberg limit scaling can be achieved for parameter estimation, where $\Delta\beta \propto 1/N$; and 2) the resulting sensing protocol works for other sensing tasks that only extract partial information about β. The intuition is as follows: recall that the key feature of bosonic cat-state sensing is producing a fine-grained interference pattern in phase space that is sensitive to the displacement signal. If the N incoherent repetitions of the cat-state sensing protocol can be concatenated together into a *single-shot coherent protocol* which coherently manipulates the phase space interference pattern beyond that produced by the simple cat-state interferometer, then the coherent sensing state can be made sensitive to the partial information that we seek from the signal. In the next section, we give a construction of a novel QSP interferometer that circumvents the above two limitations and achieves HL-like behavior for decision problems.

III. QUANTUM SIGNAL PROCESSING INTERFEROMETRY

Before presenting the QSPI construction, we first formulate a theory of bosonic QSP by alternating single-qubit rotations with controlled-displacement operations in Sec. III A and show how to utilize this bosonic QSP approach as the basic building block to produce general sensing algorithms. Building upon the bosonic QSP theory for polynomial transformations of quadrature operators as well as the cat state sensing protocol above, we define and construct a novel QSP interferometer on hybrid qubit-oscillator platforms and present a new QSPI

Theorem in Sec. III B. Detailed analysis of the behavior of the QSP interferometer for a displacement operator is discussed in Sec. III C.

A. Bosonic QSP Formalism

Coupling a bosonic oscillator to a qubit is a useful approach for achieving universal control of the oscillator [43]. It has been shown that simple Jaynes-Cummings type interactions can achieve universal control on an arbitrary low-energy d-dimensional subspaces of an oscillator [44, 45]. By using an alternative dispersive coupling, universal control on oscillators has also been demonstrated using the echo-controlled displacement operator [41]. Here, we draw a connection between these control protocols with quantum signal processing to develop a bosonic QSP formalism as a basic building block for the rest of the paper.

Quantum signal processing relies on two components: 1) a block-encoding of the signal operator; and 2) the ability to impart an arbitrary phase shift to the block-encoded operator. Block-encoding simply means embedding the target operator inside a known and accessible subspace of a unitary matrix. Methods for block-encoding on qubit devices are mostly limited to linear combination of unitaries [46, 47], and block-encoding of a general Hamiltonian seems to be difficult. It might thus seem that such block-encoding will be especially challenging in our case, as we need to block-encode an entire oscillator (with infinite dimension) into a unitary matrix in order to perform QSP on the oscillator. Surprisingly, some physical interactions between quantum systems can provide natural block-encodings of one system in the basis of the other for qubit-oscillator systems, as is stated formally in Lemma 1.

Lemma 1 (Qubitization of a Bosonic Mode via Qubit-oscillator Physical Interaction). *Coupling between a qubit Pauli operator σ_z and a bosonic mode's quadrature operators, $h(\hat{x}, \hat{p})$, naturally block-encodes the bosonic mode's unitary evolution operator $\omega(\hat{x}, \hat{p}) = e^{-ih(\hat{x}, \hat{p})t}$.*

The above statement immediately follows if we write the resulting unitary under the representation of the qubit's $SU(2)$ matrix,

$$W_z := e^{-ih(\hat{x}, \hat{p})\sigma_z t} = \begin{bmatrix} \omega(\hat{x}, \hat{p}) & 0 \\ 0 & \omega^{-1}(\hat{x}, \hat{p}) \end{bmatrix}. \quad (7)$$

Note that the choice of σ_z here is only a convention, and any coupling can always be rotated into the σ_z representation. Also, note that $\omega(\hat{x}, \hat{p})$ is an *operator* on the oscillator rather than a complex number.

Now, given the qubitization of a bosonic mode, we are ready to state a bosonic quantum signal processing theorem that summarizes the achievable polynomial

transformations on the quadrature operator $\omega(\hat{x}, \hat{p})$, as defined in Lemma 1.

Theorem 2 (Bosonic Quantum Signal Processing). *The following quantum circuit parameterized by $\vec{\theta} = \{\theta_0, ..., \theta_d\}$ achieves a block-encoding of a degree-d Laurent polynomial transformation on $\omega(\hat{x}, \hat{p})$ as $F(\omega)$*

$$Q_{\vec{\theta}}(\omega) = e^{i\theta_d \sigma_x} \prod_{j=0}^{d-1} W_z e^{i\theta_j \sigma_x} = \begin{bmatrix} F(\omega) & iG(\omega) \\ iG(1/\omega) & F(1/\omega) \end{bmatrix},$$

$$(8)$$

where (setting $t = 1$ for simplicity)

$$F(\omega) = \sum_{n=-d}^{d} f_n \omega^n = \sum_{n=-d}^{d} f_n e^{-ih(\hat{x},\hat{p})n} := f(\hat{x}, \hat{p}), \quad (9a)$$

$$G(\omega) = \sum_{n=-d}^{d} g_n \omega^n = \sum_{n=-d}^{d} g_n e^{-ih(\hat{x},\hat{p})n} := g(\hat{x}, \hat{p}). \quad (9b)$$

for $n = \{-d, -d + 2, -d + 4, ..., d\}$, $f_n, g_n \in \mathbb{R}$, $F(\omega)F(1/\omega) + G(\omega)G(1/\omega) = 1$, and $h(\hat{x}, \hat{p})$ is an analytical function of the bosonic mode's quadrature operators. Inversely, given $F(\omega)$ in Eq. (9a) and $F(\omega)F(1/\omega) < 1$, there exists $\vec{\theta} = \{\theta_0, ..., \theta_d\}$ such that the construction in Eq. (8) block-encodes $F(\omega)$.

The proof of Theorem 2 follows from the normal QSP proof on single qubit [28] or the periodic function formulation [48] once $Q_{\vec{\theta}}(\omega)$ is expanded under the infinite sets of eigenstates of $h(\hat{x}, \hat{p})$. A detailed proof can be found in App. A. We note that despite the similarity to single-qubit QSP, bosonic QSP is formally an infinite-dimensional theorem.

In general, $h(\hat{x}, \hat{p})$ can be any physically realizable Hamiltonian of the oscillator (i.e., not only finite degree polynomials but also analytic functions). To the lowest order, $h(\hat{x}, \hat{p})$ can be a linear function of $\hat{x}$ and $\hat{p}$, which generates a displacement in the phase space: $h(\hat{x}, \hat{p}) = \alpha \hat{a}^\dagger - \alpha^* \hat{a}$. Coupling h to a qubit Pauli operator generates a qubit-controlled displacement. Consider the special case where a simple qubit-oscillator coupling naturally arises on cQED hardware [49] or in trapped ions [50]; we have $h(\hat{x}, \hat{p})t = -\kappa \hat{x}$, where t denotes the duration of the qubit-oscillator interaction or coupling, which generates a displacement operator to boost the oscillator momentum by an amount of κ. From Lemma 1, it is readily realized that the physical dynamics generated from this coupling Hamiltonian form a block-encoding of the oscillator operator $\omega := e^{i\kappa \hat{x}}$. Combined with Theorem 2, we have

$$F(\omega) = \sum_{n=-d}^{d} f_n e^{i\kappa \hat{x}n} := f(\hat{x}), \quad (10a)$$

$$G(1/\omega) = \sum_{n=-d}^{d} g_n e^{i\kappa \hat{x}n} := g(\hat{x}), \quad (10b)$$

where $n = \{-d, -d + 2, -d + 4, ..., d\}$, and d is the degree of QSP, as specified in Theorem 2. The achievable functions and parity constraints upon $Q_{\vec{\theta}}(\omega)$ for $\omega \in \mathbb{C}$ are described in [48]. Note that in this case ω is a unitary operator that maps oscillator position $x \in (-\infty, \infty)$ to the complex unit circle, so $f(\hat{x})$ and $g(\hat{x})$ are periodic functions with a period $T_x = \frac{2\pi}{\kappa}$. For an integer m:

$$f(\hat{x} + mT_x) = f(\hat{x}), \quad (11a)$$

$$g(\hat{x} + mT_x) = g(\hat{x}). \quad (11b)$$

The overall construction of the bosonic QSP circuit from Theorem 2 is shown in Fig. 2, where the conditional displacement operator and single qubit rotations are performed repeatedly. Since this construction performs an arbitrary degree-d real Laurent polynomial on ω with definite parity, it follows that the resulting functions $f(\hat{x})$ and $g(\hat{x})$ have flexibility to achieve a wide class of functions on $\hat{x}$ in the interval $[-\frac{\pi}{\kappa}, \frac{\pi}{\kappa}]$ that admit at most a degree-d Fourier expansion, as in Eq. (9a) and Eq. (9b). Note that the numerical and experimental realization of such conditional displacements in Ref. [41] for universal control of oscillators provides an example of the expressivity of such a bosonic QSP construction. The ability to obtain such nonlinear transformations on oscillator quadrature operators forms the basis of the QSP interferometry, as we will discuss next.
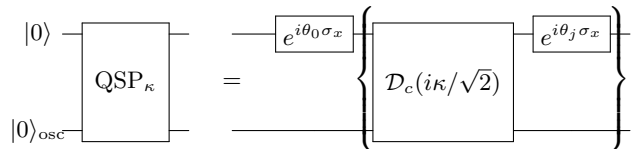

FIG. 2. A bosonic QSP circuit composed of single-qubit rotations and controlled displacement operations, where the form of $\mathcal{D}_c(i\kappa/\sqrt{2})$ is given in Eq. (2) . The gates inside the bracket are repeated d times for different θ_j $(j = 1, 2, \cdots, d)$ in order to obtain a degree-d Laurent polynomial.

B. QSP Interferometry

Building on the ability to perform polynomial transformations on a bosonic oscillator's quadrature operators using QSP in Sec. III A and Theorem 2, we construct a QSP interferometry (QSPI) protocol in this section by combining two bosonic QSP sequences.

A QSP interferometry protocol is defined as follows:

Definition 2 (Degree-d Quantum Signal Processing Interferometry (d-QSPI)). *Given an underlying bosonic signal unitary $S_\beta = e^{ih_\beta(\hat{x},\hat{p})}$, where $h_\beta(\hat{x}, \hat{p})$ is a finite-degree Hermitian polynomial of the quadrature operators $\hat{x}, \hat{p}$ parameterized by $\beta \in \mathbb{R}$, a degree-d quantum signal processing interferometry (d-QSPI) protocol for S_β is defined as the protocol in Fig. 1c, or $Q_{\vec{\theta}}^{-1}(\omega)S_\beta Q_{\vec{\theta}}(\omega)$, where $Q_{\vec{\theta}}(\omega)$ is given by Eq. (8). Furthermore, we define*

the joint qubit-oscillator state created by $Q_{\vec{\theta}}(\omega)$ as the QSPI sensing state $|\tilde{Q}\rangle = Q_{\vec{\theta}}(\omega)|\downarrow\rangle \otimes |0\rangle_{\text{osc}}$.

It is readily recognized that the QSPI protocol described in Definition 2 is a simple generalization of the usual cat-state interferometry protocol, where the cat-state preparation is replaced by an arbitrary bosonic QSP transformation. Each d-QSPI protocol is entirely characterized by the angle sequence $\vec{\theta}$.

As an interferometer, the unitary operation realized by a d-QSPI must be a linear combination of many elementary unitaries, where the interference among them performs some desired quantum sensing task. To make the interferometry aspect of QSPI more vivid and to reveal how individual unitaries (or "paths") interfere, it is useful to identify what such elementary unitaries look like in QSPI. Because each matrix element of the bosonic QSP constructed in Eq. (8) is a linear combination of ω^n for different $n \in [-d, d]$, we define a *QSPI elementary transformation* on the signal S_β under the basis ω^n:

Definition 3 (QSPI Elementary Transformation). *An elementary QSPI transformation $S_{\beta,nm}(\hat{x}, \hat{p})$ on S_β is defined as follows:*

$$S_{\beta,nm}(\hat{x}, \hat{p}) := \omega^{-n} S_\beta \omega^m, \qquad (12)$$

for some $\omega = e^{-ih(\hat{x}, \hat{p})}$ acting on a bosonic mode and for integers n, m.

From a basis-set-expansion point of view, Eq. (12) is equivalent to expanding the unknown operator S_β under the basis set $\{\omega^n\}$, where $S_{\beta,nm}(\hat{x}, \hat{p})$ is simply the resulting matrix element (despite its infinite-dimensional nature). In the special case of $\omega = e^{i\kappa\hat{x}}$, Eq. (12) can be viewed as a plane-wave expansion of S_β for a set of discrete reduced momenta nk for integer n, which is similar to the k-point sampling technique in the numerical study of periodic solid-state systems [42], where k determines the low-energy cutoff, while the upper limit of n dictates the high-energy cutoff. We will see in the following that this high-energy cutoff is directly related to the QSP degree d that is being used in our construction.

With the elementary transformation defined, we are now ready to present the QSPI transformation theory that describes how QSPI acts as an interferometer:

Theorem 3 (QSP Interferometry Theorem). *A d-QSPI protocol for a bosonic signal unitary S_β performs a transformation to S_β such that the resulting unitary is a linear combination of d^2 elementary transformations $S_{\beta,nm}(\hat{x}, \hat{p})$ as defined in Def. 3*

$$Q_{\vec{\theta}}^{-1}(\omega) S_\beta Q_{\vec{\theta}}(\omega) = \sum_{n,m=-d}^{d} C_{nm} S_{\beta,nm}(\hat{x}, \hat{p}), \qquad (13)$$

where C_{nm} is a complex coefficient matrix defined from the original QSP coefficients by

$$C_{nm} = \begin{bmatrix} f_n f_m + g_{-n} g_{-m} & i(f_n g_m - g_{-n} f_{-m}) \\ i(f_{-n} g_{-m} - g_n f_m) & g_n g_m f_{-n} f_{-m} \end{bmatrix}, \quad (14)$$

which serves as a complex weight to its associated elementary transformation $S_{\beta,nm}$ in order to produce the desired interference.

The proof of the theorem follows by direct multiplication of the left-hand side of Eq. (13). $\square$

The right-hand side of Eq. (13) is a sum of d^2 terms, each weighted by a complex coefficient matrix C_{nm}, as defined in Eq. (14); this readily reveals that the resulting unitary of a d-QSPI protocol is essentially a giant interferometer of d^2 elementary components. Note that each element of C_{nm} is always quadratic in terms of f and g (either a product of two f or two g with different subscripts); this is simply a consequence of the fact that the QSP sensing state $|\tilde{Q}\rangle$ prepared in Fig. 1c is perturbed by S_β before interfering with itself. In this fashion, the original QSP coefficients f_n, g_n can be tuned such that the desired interference pattern is produced by the protocol for any quantum sensing purpose. Note that there is no approximation, such as truncating the dimension of the infinite dimensional oscillators, in our formalism, since we explicitly work with the oscillator quadrature operators, and the physical regularization of the infinite dimensional transformation is provided by a finite energy initial state (for example, a vacuum state).

Theorem 3 characterizes at the operator level how QSPI works, but it is not clear what or how much information can be extracted from the entire protocol via measurement. We discuss the measurement aspect in the following.

Just as in any interferometry protocol, we are interested in extracting information about S_β by performing some *measurement* after the protocol, where the measurement outcome contains information about the parameter β. It is possible to measure oscillators directly using homodyne/heterodyne detection or by performing a photon-number-resolved measurement. Such measurements will often provide *local* information on the phase-space distribution of the oscillator wave function. Alternatively, it is much easier (and typically faster) to measure the ancilla qubit directly. Such a qubit measurement implies a partial trace over the bosonic quadrature operator and therefore will provide useful *global* information about the oscillator. Extracting such global information is crucial to performing decision-making regarding the underlying signal parameter β, as we will see in Sec. IV A. For the ease of discussion, we define the QSPI response function as follows:

Definition 4 (QSPI Response Function). *A QSPI response function is defined as the probability distribution over the signal parameter β after a projective measurement on the ancilla qubit as $\mathbb{P}(\beta) = ||\langle\phi_1|Q_{\vec{\theta}}^{-1}(\omega)S_\beta Q_{\vec{\theta}}(\omega)|\phi_0\rangle|0\rangle_{\text{osc}}||^2$, where $|\phi_0\rangle$ and $|\phi_1\rangle$ are the initial and final state of the ancilla qubit and the oscillator is assumed to start from vacuum $|0\rangle_{\text{osc}}$.*

QSPI response functions, or simply the response functions, as defined in Definition 4, characterize the

complicated interference pattern between two oscillator states that are perturbed by S_β. The signature of such interference is cast onto the qubit measurement probability. In our case, the unitary channel that we wish to distinguish is a displacement of the oscillator perpendicular to W_z's displacement direction. The effect of the displacing signal S_β can be understood as convolving the QSP sensing state $|\tilde{Q}\rangle$ with a shifted version of itself. Thus, for an optimal choice of the QSP polynomial, we expect to be sensitive to a certain range of displacements. This protocol takes Ramsey interferometry protocols as in [10, 15] as inspiration. In fact, Eq. (5) in Sec. II B can be viewed as a simple response function for cat-state sensing, since it can be realized by a degree-1 QSPI protocol, as we will see in the next section.

C. QSPI Protocols for Displacement Sensing

We will examine the outcome for the qubit state in our generalized QSP sensing protocol for displacement sensing in Sec. III C 1, and use a degree-1 case as an example to connect to the cat state sensing protocol in Sec. III C 2.

1. General Theory of QSPI Displacement Sensing

We shall drop $\vec{\theta}$ subscripts from Q from here on for simplicity. The sensing sequence, also from Fig. 1c, is given by:

$$U(\beta, \omega) = Q^{-1}(\omega)S_\beta Q(\omega), \tag{15}$$

where $Q^{-1}(\omega) = Q^\dagger(1/\omega)$. Using Eq. (3), we may rewrite Eq. (15) as

$$U(\beta, \omega) = Q^{-1}(\omega)S_\beta Q(\omega) = S_\beta Q^\dagger(1/\omega')Q(\omega), \tag{16}$$

where

$$\omega' = \omega e^{-i\kappa\beta} = e^{i\kappa(\hat{x}-\beta)}. \tag{17}$$

The right-hand side of Eq. (16) reveals a key insight: the total QSPI protocol reduces to a product of $Q^\dagger(1/\omega')Q(\omega)$ (up to an irrelevant global phase S_β), which is a QSP sequence interfering with a shifted version of itself $\omega \to \omega'$ by a constant phase $e^{-i\kappa\beta}$, as defined in Eq. (17). It is this β-dependent shift that allows the extraction of useful information on β from the interferometry.

In order to find the response function for the probability of measuring the qubit in the ground state after the sensing protocol, we must integrate over the probability distribution in phase space. Let us denote the upper left matrix element of U as $U_{00} = e^{i\beta\hat{p}}[f(\hat{x} - \beta)f(-\hat{x}) + g(\hat{x} - \beta)g(-\hat{x})]$, then the measurement probability of the qubit being at state $|\downarrow\rangle$ is

$$\mathbb{P}(M = \downarrow | \beta)$$
$$= || \langle\downarrow| Q^{-1}SQ |\downarrow\rangle |0\rangle_{\text{osc}} ||^2$$
$$= \langle 0|_{\text{osc}}(U_{00})^\dagger U_{00} |0\rangle_{\text{osc}}$$
$$= \int_{-\infty}^{\infty} dx \, |[f(-x+\beta)f(x) + g(x-\beta)g(-x)] \, \psi_0(x)|^2. \tag{18}$$

where $\psi_0(x) = \pi^{-1/4}e^{-x^2/2}$ is the vacuum state of the oscillator, and we have used real numbers x as the argument of $f(\cdot)$ and $g(\cdot)$ since everything has been written under the position representation. Thus, $\mathbb{P}(M = \downarrow | \beta)$ is a function of our signal parameter β and the original QSP phase angles. We may now tailor the shape of the QSP Laurent polynomial such that the qubit response $\mathbb{P}(M = \downarrow | \beta)$ scales optimally versus β.

Using the Laurent polynomial expressions from Eq. (9a) and Eq. (9b) and explicitly evaluating the integration with respect to x, we can alternatively write Eq. (18) as a series sum

$$\mathbb{P}(M = \downarrow | \beta) = \sum_{s=-d}^{d} c_s v(\beta)^s \tag{19}$$

for $v(\beta) = e^{i(2\kappa)\beta}$ and $c_s \in \mathbb{R}$ being a function of κ

$$c_s = \sum_{n,n',r=-d}^{d} (f_n f_{n'} + g_n g_{n'})$$
$$\times (f_{n+2s}f_{n'+2r} + g_{n+2s}g_{n'+2r})e^{-\kappa^2(r-s)^2} \tag{20}$$

where n, n' are either all odd or all even depending on the parity of d. It follows that the response function of the qubit $\mathbb{P}(M = \downarrow | \beta)$ is a degree-d Laurent polynomial with respect to the new "signal" operator $v(\beta, \kappa) = e^{i(2\kappa)\beta}$. See Appendix B for a proof.

FIG. 3. Pictorial illustration of how in the bosonic QSP interferometric protocol, the qubit measurement enacts a duality between a polynomial transformation on the bosonic quadrature operators and a polynomial transformation on the sensing parameter β via QSPI.

Therefore, apart from parity and normalization constraints, we may design the qubit response $\mathbb{P}(M = \downarrow | \beta)$ by choosing f_n and g_n such that we approach the desired Fourier series of a function of β. This relationship also reveals an interesting duality between the QSP polynomial transformation on phase space quadrature and the polynomial transformation on the signal parameter β in the response function, which is highlighted in Fig. 3 and summarized as Theorem 4.

Theorem 4 (QSPI for Displacement Sensing). *Given a degree-d QSPI protocol with the block-encoded quadrature operator $\hat{w} = e^{i\kappa\hat{x}}$ (periodic with a period of $[-\frac{\pi}{\kappa}, \frac{\pi}{\kappa}]$ with respect to x), a degree-d response function $\mathbb{P}(v) := \sum_s c_s v^s$, with $v = e^{i(2\kappa)\beta}$ as its argument, is well-defined where $\beta \in [-\frac{\pi}{2\kappa}, \frac{\pi}{2\kappa}]$. Conversely, given a degree-d real Laurent polynomial transformation (defined in Eq. (19) with c_s as its coefficients) on $v = e^{i(2\kappa)\beta}$ where $\beta \in [-\frac{\pi}{2\kappa}, \frac{\pi}{2\kappa}]$ as the desired response function that satisfies the following necessary conditions,*

$$\sum_{s=-d}^{d} c_s = 1, \quad c_s = c_{-s}, \tag{21a}$$

$$0 \leq \sum_s c_s v(\beta)^s \leq 1, \tag{21b}$$

there exists a d-QSPI protocol as in Fig. 1c that realizes the desired response function.

We will now sketch a proof of the above theorem. From [48], we know for a given QSPI protocol characterized by $\vec{\theta}$ that $f(x)$ and $g(x)$ are well-defined, and thus the forward direction of Theorem 4 is trivial.

On the other hand, it is in general challenging to provide sufficient conditions for response functions such that they can be realized by the QSPI protocol using a set of phase angles $\vec{\theta}$. Here for the reverse direction of Theorem 4, we resort to only necessary conditions on the response function.

Because the response function is necessarily a probability on the qubit and involves a integral over the bosonic coordinates, there are additional constraints on the response function. First, from the response function's relevant parity and normalization constraints on c_s as defined in Eq. (19), Eq. (21a) can be derived. Secondly, beyond the parity and normalization constraints, we must also impose an additional constraint on possible sets of c_s due to the response function being a probability, which requires Eq. (21b) to be satisfied for all $\beta \in \mathbb{R}$. □

Let us make additional remarks on the reverse direction of Theorem 4. The reason that it is challenging to ascertain a set of sufficient conditions on the response function is due to the nonlinear transformation of F, G in Eq. (18). Inverting the system of polynomial equations in Eq. (20), even in the large κ limit where decay coefficients vanish, appears analytically intractable. From our construction in Eq. (9), it can be inductively shown that $f_{-d} = g_d = 0$, and from [48], $F(\omega)$ determines $G(\omega)$ up to $\omega \mapsto 1/\omega$. Thus, for fixed κ, we may reduce Eq. (20) to a system of d independent equations with d unknowns, but searching for solution sets of such polynomial equations is difficult and often infeasible analytically.

2. Example: Cat State Sensing

For the degree $d = 1$ case, and $\{\theta_0, \theta_1\}$ as the QSP phase angles, the QSPI response function is

$$\mathbb{P}(M =\downarrow |\beta) = c_0 + c_1 v + c_{-1} v^{-1} \tag{22}$$

where

$$c_0 = \cos^4(\theta_0) + \sin^4(\theta_0) \tag{23}$$

$$c_1 = c_{-1} = \cos^2(\theta_0) \sin^2(\theta_0). \tag{24}$$

Evidently, this is a degree-1 Laurent polynomial of the argument $v = e^{i(2\kappa)\beta}$, where all of the polynomial coefficients are real. Also, we note that the measurement probability is independent of θ_1 (or, in general, θ_d for a d-QSPI protocol) per the construction. Furthermore, by choosing $\theta_0 = \pi/4$, we recover exactly the cat state sensing protocol with $\mathbb{P}(M =\downarrow |\beta) = \cos^2(\kappa\beta)$. Thus, the cat state sensing protocol is indeed a special case of a 1-QSPI protocol!

IV. BINARY DECISION-MAKING USING QSPI

Now, we have established the QSPI protocol and its response function as a polynomial transformation of the signal. To demonstrate its potential for general sensing tasks, we derive an explicit expression for the response function for a binary decision problem on the displacement parameter in Sec. IV A and analyze analytically the decision quality and sensing complexity in Sec. IV B.

A. Binary decision for displacement sensing

For a classical binary decision using measurement of a single qubit, we want the QSPI response function to be either 1 or 0 depending on the value of the signal displacement relative to β_{th}. In particular, one such target qubit response function is the step function

$$P_{\text{ideal}}(\beta) = \begin{cases} 1, & 0 \leq |\beta| < \beta_{\text{th}} \\ 0, & \beta_{\text{th}} < |\beta| \leq \frac{\pi}{2\kappa}. \end{cases} \tag{25}$$

If such an ideal qubit response function is realized, then the binary decision sensing protocol has no error. However, in practice, only a finite-degree polynomial approximation to this function is available and lead to decision errors. In the following, we give basic definitions to quantify the decision errors.

For ease of discussion, Fig. 4 plots the ideal response function (red) in contrast to a typical polynomial approximation generated by the QSPI protocol (black) as a function of the underlying displacement β. The approximated response function features a steep yet finite slope centered about β_{th}. There are usually some small

oscillatory patterns for small β and for $\beta_{\text{th}} < |\beta| < \frac{\pi}{2\kappa}$. Deviations of $P_{\text{approx}}(\beta)$ from $P_{\text{ideal}}(\beta)$ across the entire range of $\left[-\frac{\pi}{2\kappa}, \frac{\pi}{2\kappa}\right]$ quantify the overall probability of making the wrong decision. We define the following quantity as *decision error density*:

$$p_{\text{err}}(\beta_{\text{th}}, \kappa) = \frac{\kappa}{\pi} \int_{-\frac{\pi}{2\kappa}}^{\frac{\pi}{2\kappa}} |P_{\text{approx}}(\beta) - P_{\text{ideal}}(\beta)| \, d\beta$$

$$= p_{\text{err,FN}}(\beta_{\text{th}}) + p_{\text{err,FP}}(\beta_{\text{th}}). \quad (26)$$

This quantity can be split into two contributions according to β_{th} as follows:

$$p_{\text{err,FN}}(\beta_{\text{th}}) = \frac{2\kappa}{\pi} \int_0^{\beta_{\text{th}}} (1 - P_{\text{approx}}(\beta)) \, d\beta, \quad (27a)$$

$$p_{\text{err,FP}}(\beta_{\text{th}}) = \frac{2\kappa}{\pi} \int_{\beta_{\text{th}}}^{\pi/2\kappa} P_{\text{approx}}(\beta) d\beta. \quad (27b)$$

The former, $p_{\text{err,FN}}(\beta_{\text{th}})$, defined in Eq. (27a), is the false-negative (FN) error (also called Type-II error in hypothesis testing) and is indicated by the grey region in Fig. 4, while the latter, $p_{\text{err,FP}}(\beta_{\text{th}})$, defined in Eq. (27b), is the false-positive (FP) error (Type-I error) and is highlighted in orange in Fig. 4 [51]. Our goal in designing the response function is to find QSP phase angles that minimize the total decision error in Eq. (26).
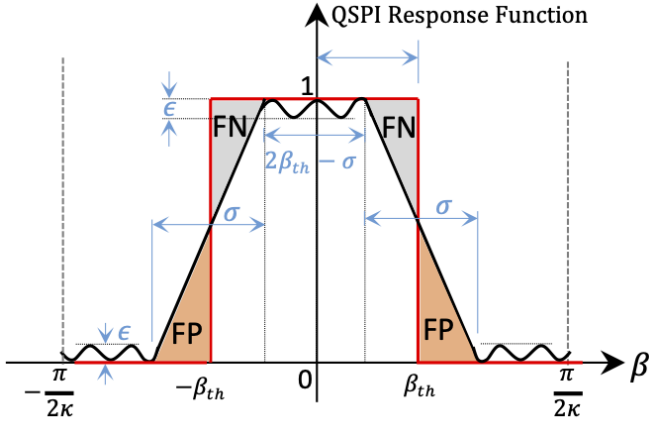

FIG. 4. Schematic of erroneous decision making probability (from the response function) as the difference between the ideal response function (solid red) and a polynomial approximated response function (solid black). For an event defined as "the displacement is below threshold β_{th}", the integrated erroneous probability is composed of two parts: i) missing the event while it actually happened (false-negative, FN, Type-II error, grey-shaded area), ii) reporting the event when it did not happen (false-positive, FP, Type-I error, orange-shaded area). Note that the effective detection signal range is $\left[-\frac{\pi}{2\kappa}, \frac{\pi}{2\kappa}\right]$.

Substituting Eq. (19) into Eq. (26), the error probability can be written explicitly as

$$p_{\text{err}}(\beta_{\text{th}}, \kappa) = \sum_{s=-d}^{d} c_s H_s(\beta_{\text{th}}, \kappa), \quad (28)$$

where we have defined

$$H_s(\beta_{\text{th}}, \kappa) = \frac{2\kappa\beta_{\text{th}}}{\pi} + \text{sinc}(\pi s) - \frac{4\kappa\beta_{\text{th}}}{\pi}\text{sinc}(2\kappa s\beta_{\text{th}}) \quad (29)$$

as a function of $(\beta_{\text{th}}, \kappa)$, and the definition of c_s is given in Eq. (20). Eq. (28) is the central metric for the binary decision problem in displacement sensing.

Additionally, note that κ and β_{th} always appear together in Eq. (29) as a product, which suggests there is a scale-invariance in the definition of H_s in the sense that the displacement length scale can be measured in units of $1/\kappa$ and only this relative length scale with respect to $1/\kappa$ is meaningful. Toward this end, we introduce a dimensionless parameter η to quantify $\beta_{\text{th}} = \eta\frac{\pi}{\kappa}$. It is evident that the dynamic range for the signal β will be $\eta \in [-0.5, 0.5]$, as is suggested by the horizontal axis of Fig. 4. However, the dependence of the coefficients c_s on κ in Eq. (B8) means p_{err} is still κ-dependent which in turn suggests the optimal sensing QSPI phase angles depend on κ.

1. Limitation of Cat State for Decision Making

As we have seen in Sec. III C 2 and in Fig. 1b, the cat-state sensing protocol corresponds to a degree $d = 1$ QSPI. It has also been shown in Eq. (6) in Sec. II B that the cat state sensing protocol achieves the celebrated Heisenberg limit sensing for parameter estimation. In this section, we will characterize the performance of cat-state sensing protocol for *decision-making* and reveal its limitations in this regard.

For degree $d = 1$ QSPI, the integrated probability of making the wrong decision per unit signal can be calculated as

$$p_{\text{err}} = \frac{1}{4\pi} \Big[\sin(2\beta_{\text{th}}\kappa - 4\theta_0) + \sin(2\beta_{\text{th}}\kappa + 4\theta_0) \quad (30)$$

$$+ (\pi - 4\beta_{\text{th}}\kappa)\cos(4\theta_0) - 4\beta_{\text{th}}\kappa - 2\sin(2\beta_{\text{th}}\kappa) + 3\pi \Big]. \quad (31)$$

We would like to minimize p_{err} overall by choosing θ_0 appropriately. The global minimum is found to be the following when $\theta_0 = \pi/4$ (regardless of β_{th} and κ):

$$p_{\text{err}}|_{\theta_0=\frac{\pi}{4}} = \frac{1}{2} - \frac{\sin(2\kappa\beta_{\text{th}})}{\pi}. \quad (32)$$

On the other hand, supposing that we perform no rotation on the qubit, or $\theta_0 = 0$, we obtain $\mathbb{P}(M = \downarrow | \beta) = 1$, which gives

$$p_{\text{err}}|_{\theta_0=0} = 1 - \frac{2\kappa\beta_{\text{th}}}{\pi}. \quad (33)$$

This makes sense because this scenario is equivalent to making a decision that the displacement is always below β_{th}, and therefore there is only false positive error and
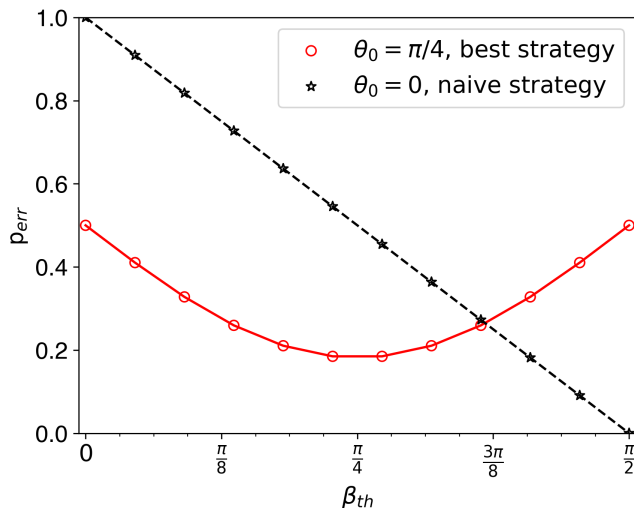
FIG. 5. The probability of making wrong decision versus the decision threshold β_{th}. Data shown for a binary decision of displacement sensing using degree-1 bosonic QSP with $\kappa = 1$, comparing the best ($\theta_0 = \pi/4$, red circle) and the naive ($\theta_0 = 0$, black star) sensing protocol.

the error probability should decrease as β_{th} is increased. Moreover, when $\beta_{\text{th}} = \frac{\pi}{2\kappa}$, which is on the boundary of the sensing range, p_{err} drops to zero.

A comparison of the scaling of p_{err} versus β_{th} between the best decision $\theta_0 = \pi/4$ and the ignorant decision $\theta_0 = 0$ is shown in Fig. 5. It can be seen that the optimal sensing strategy significantly reduces p_{err} when $\beta_{\text{th}} < \beta_{\text{th}}^*$, while it performs worse than the naïve guess for $\beta_{\text{th}} > \beta_{\text{th}}^*$ where $\beta_{\text{th}}^* = \frac{\chi}{2\kappa}$ for χ being the solution to the transcendental equation $\frac{\pi}{2} - x + \sin(x) = 0$. The optimal sensing protocol works best for $\beta_{\text{th}} = \frac{\pi}{4\kappa}$, where it gives $p_{\text{err}} = \frac{1}{2} - \frac{1}{\pi}$. This simple example also demonstrates the non-trivial complexity of decision problems even for the most simple decision problems.

The above analysis also reveals that the minimum p_{err} achieved by the cat-state sensing protocol is always a constant regardless of the value of the displacement κ or the size of the cat state for a threshold $\beta_{\text{th}} = \frac{\pi}{4\kappa}$. This behavior is in drastic contrast with parameter estimation tasks, where a larger cat state will have finer interference fringes in phase space and therefore achieve Heisenberg limit estimation accuracy for very small displacements (Eq. (6) of Sec. II B). An intuitive reason why decision making with a larger cat-state does not help is that the integration in Eq. (26) smears out the local information in the oscillator wave function (e.g., the fine interference fringes), meaning that globally, a larger cat-state behaves the same as a smaller cat-state for the binary decision.

B. Algorithmic Complexity for Binary Decision

Given the definition of the decision error density $p_{\text{err}}(\beta_{\text{th}}, \kappa)$, in this section, we would like to understand some fundamental limits on how $p_{\text{err}}(\beta_{\text{th}})$ scales with the degree of the QSP. This determines the algorithmic complexity of making a high-quality binary decision using a QSPI protocol.

To do this, we first construct a composite function that exactly reproduces $P_{\text{ideal}}(\beta)$ (red trace in Fig. 4) in the relevant sensing range of $[-\frac{\pi}{2\kappa}, \frac{\pi}{2\kappa}]$. In particular, consider

$$P_{\text{ideal}}^{\text{sign,sin}}(\beta) = \frac{\text{sign}\left[\sin(\kappa(\beta_{\text{th}} - \beta))\right] + \text{sign}\left[\sin(\kappa(\beta_{\text{th}} + \beta))\right]}{2},$$
(34)

where $\text{sign}(\cdot)$ is the sign function. We use the superscript $^{\text{sign,sin}}$ to distinguish the current construction from other possible constructions for $P_{\text{ideal}}(\beta)$.

With this, it can be shown (Appendix D) that to achieve a target faulty decision probability p_{err}, the required QSP polynomial degree d to approximate $P_{\text{ideal}}^{\text{sign,sin}}(\beta)$ must have

$$d \propto \frac{1}{\kappa p_{\text{err}}} \log\left(\frac{1}{\kappa p_{\text{err}}}\right).$$
(35)

For small p_{err}, $\log\left(\frac{1}{p_{\text{err}}}\right) \ll \frac{1}{p_{\text{err}}}$. Therefore, the total faulty decision probability can be solved from Eq. (35)

$$p_{\text{err}} \propto \frac{1}{\kappa d} \log(d).$$
(36)

Recall that in a standard parameter estimation task, Heisenberg-limit scaling is defined when the standard deviation for estimating the underlying parameter scales as $1/t$ where t is the total time for the sensing protocol (also see discussions in Sec. II B). Here for our case of binary decision making, analogous to parameter estimation, Eq. (36) suggests that our QSPI protocol can achieve a similar Heisenberg-limit scaling where the probability of making the wrong decision decreases as $1/d$ (up to a logarithmic factor of $\log(d)$) where d is proportional to the runtime of the sensing protocol. More strictly speaking, the appearance of the $\log(d)$ factor in Eq. (36) will make the actual scaling slightly worse than the Heisenberg limit, as is corroborated by numerical evidence in Sec. VI.

V. PARAMETER ESTIMATION FROM QUANTUM DECISIONS

Among general quantum sensing tasks in addition to decision making, another important class of problems is to estimate a parameter (or multiple parameters) up to a given precision. In Sec. IV, it has been shown that Heisenberg-limit scaling can be achieved in determining

whether a displacement signal is below or above a given threshold in the single-sample limit. One natural question is whether such decision making protocol can be combined with classical search or majority voting techniques to efficiently estimate a given displacement parameter β to high precision ϵ.

In this section, we show that this is possible by repeatedly querying the binary decision protocol in Sec. IV A. In particular, Sec. V A presents a naive classical binary search strategy with a finite success probability. Sec. V B then describes a way to exponentially suppress the failure probability using majority voting.

A. Naive Classical Binary Search Protocol

Suppose that we have a displacement channel that results in displacement by some unknown $\beta \in [0, R]$, we would like to know the value of β within error ϵ using the quantum decision protocol in previous sections. How long (in terms of QSP degree and queries to the displacement signal) will it take?

We may approach this task by a naive binary search method, which subdivides the search space each step by performing a binary decision using an approximate threshold function in Sec. IV A, to determine whether β is above or below the threshold. This process may continue with a different threshold each time until finally we pin down the value of β. Obviously, if a perfect threshold function (red trace in Fig. 4) is provided each time, this reduces to a purely classical search problem, and it is known that for N total bisections, we can determine β to a precision of $\delta = R/2^N$. Therefore, to achieve fixed accuracy δ on β, the required number of queries to the perfect threshold function will be

$$N_{\text{query,ideal}} = \log_2(R/\delta), \qquad (37)$$

which demonstrates exponentially increased accuracy as the number of queries to the perfect threshold function increases. The entire protocol will be deterministic with unity success probability.

However in practice, due to the polynomial approximation to the ideal threshold function, there will be a non-zero probability of making the wrong decision at each step. Therefore, the overall binary search will have a finite failure probability. Moreover, the finite width in the falling edge of the qubit response function will necessarily impose a fundamental limit on how accurate the binary search can continue for given fixed QSP degree d.

To perform the binary search, the first step is to choose the relevant κ value for the controlled-displacement operator in QSP to set the upper bound on the period of the response function to at least R. Thus, we choose $\kappa = \pi/2R$. The position of the threshold can be chosen for the j-th binary search to be $\beta_{\text{th},j} = R/2^j$. Recall that the width of the falling edge of the qubit response function is $\kappa \approx p_{\text{err}}$, which means we can at most achieve an accuracy of $\delta \approx \kappa \approx p_{\text{err}}$, before subsequent thresholds lie within the falling edge of the current qubit response function (i.e., the decision protocol will become a parameter estimation problem).

Combining Eq. (37) and Eq. (36), this sets a limit on the total number of binary decision search one may perform

$$N_{\text{query,max}} \approx \log_2(\kappa dR/\log(d)), \qquad (38)$$

before the falling edge's width prevents us from making a sharp decision.

Moreover, since each binary search has a failure probability of p_{err}, the overall failure probability of the binary search protocol for a given degree-d will be

$$p_{\text{failure}} = p_{\text{err}} N_{\text{query,max}} \approx \frac{\log(d)}{\kappa d} \log_2\left(\frac{\kappa dR}{\log(d)}\right). \quad (39)$$

Therefore, a d-QSPI sensing protocol can at most estimate the displacement β to precision $\delta = \frac{1}{\kappa d}\log(d)$ with $N_{\text{query,max}}$ queries to the displacement signal with a limited success probability of $1 - p_{\text{failure}}$, where $N_{\text{query,max}}$ and p_{failure} are given by Eq. (38) and Eq. (39), respectively. After this, one can of course make further queries to reduce the uncertainty of the underlying parameter β, but this is more akin to a parameter estimation instead of a decision protocol.

B. Boost Estimation Success Probability via Majority Voting

The above search protocol has a failure probability that decreases $\sim 1/d$ as the QSP degree increases. In this section, we show that the failure probability can be suppressed exponentially as the number of samples increases.

Consider modification of the above protocol by repeating the binary decision M times during each round of search, and then using majority vote to determine the decision outcome in each search. From binomial distribution, the total probability of making the wrong decision for each round of the binary search is

$$p_{\text{err},M} \propto \sum_{m=M/2+1}^{M} \binom{M}{m} p_{\text{err}}^m (1 - p_{\text{err}})^{M-m}$$
$$\approx \frac{M!}{(M/2)!(M/2)!} p_{\text{err}}^{M/2} \qquad (40)$$

for small p_{err} (or large d). Following similar analysis, the overall failure probability of the entire binary search will be reduced to

$$p_{\text{failure},M} = p_{\text{err},M} N_{\text{query,max}}$$
$$\approx \left(\frac{4\log(d)}{\kappa d}\right)^{M/2} \log_2\left(\frac{\kappa dR}{\log(d)}\right) = O(d^{-M/2}) \qquad (41)$$

which is an exponential suppression as compared to the $1/d$ scaling in the case of single-sample decision, at the expense of a total of $N_{\text{query,max}}M$ queries to the displacement signal.

VI. NUMERICAL RESULTS AND DISCUSSIONS

Building on the fundamental theory and analytical analysis of the quantum signal processing interferometry, in this section we provide numerical evidence to support our analytical findings for binary decision making on displacement channels and to demonstrate the advantage of the QSPI for quantum sensing tasks.

A key task to construct the desired QSPI protocol is to find the corresponding QSPI phase angles $\vec{\theta}$ as in Definition 2. For a given decision problem, the existing analytic angle-finding algorithms for QSP [52, 53] cannot be directly applied in QSPI to realize the optimal response function due to reasons mentioned in Sec. III C 1. In this section, we resort to numerical optimization algorithms, which are capable of carrying out such multi-variable approximate optimization tasks on a reasonable timescale to find the QSPI angles. See Ref. [54] for the source code and related data accompanying this work. The rest of this section is organized as follows. Sec. VI A presents the response function from our numerical optimization, while Sec. VI B further exhibits the favorable Heisenberg-limit scaling for the error decision probability from these numerical solutions. In Sec. VI C, we discuss features of the Wigner function of the optimal sensing states $|\tilde{Q}\rangle$ as defined in Definition 2.

A. QSPI Phases for Binary Decisions

As discussed, we seek a QSPI protocol that generates a response function approximating a step function with sharp transitions at $\pm\beta_{\text{th}}$, as given in Eq. (25). We approximate the ideal response function via machine optimization of the phases θ_j in Eq. (8) to minimize the objective function p_{err} in Eq. (26) and Eq. (28) for different degrees d. We use the standard Nelder-Mead optimization algorithm as implemented in Python in the `scipy` optimization package with convergence defined to take place whenever either p_{err} or every QSPI rotation angle in $\vec{\theta}$ changes by at most 10^{-5} radians in a single step of optimization.

We compute the corresponding response function based on converged optimization results, and plot this as a function of β in Subfig. 6(a) for degrees $d = 1$, 5, 9, and 13, with Subfigs. 6(b) and 6(c) zoomed in for the small and large β regions, respectively. As shown in the figure, when $d = 1$, the response function simply takes the shape of a $\cos(\cdot)$ function. As the degree of the QSPI protocol increases, not only does the slope of

the falling edge become steeper, but also, more ripples are observed in the wings, as highlighted in panels (b) and (c) of Fig. 6. These ripples are a common feature for finite-degree polynomial approximations to discontinuous functions.

Furthermore, a closer observation of the response function reveals that a d-QSPI protocol has precisely $(d-1)$ local minima or maxima of its corresponding response function in the interval $[0, \frac{\pi}{2\kappa})$. This is expected because a degree-d polynomial on β has at most $(d-1)$ turning points. From a signal processing perspective, such qubit response functions serve as low-pass filters on the signal parameter β [55]. We note that filters have been widely used in classical decision-making [56], where filter functions (or impulse response) of the desired shape can be implemented as infinitely smooth analytical functions (such as the Butterworth or Chebyshev filters) or as finite-degree polynomials. The former class of filters are often called infinite impulse response because an exact realization of the response would require an infinite order polynomial, while the later are named finite impulse response. Our QSPI protocol can therefore be viewed as a quantum circuit realization of a finite impulse response (finite-degree filter) on a classical parameter β which parameterizes a quantum process (the underlying displacement signal). There is efficient classical algorithm, the Parks-McClellan algorithm, that designs optimal finite-order polynomial filters [25]. It is interesting to ask whether there exist a quantum version of the Parks-McClellan algorithm for filter design. Another question is to what extent can our QSPI protocol realize classical filters of certain degree. Sufficient conditions on Theorem 4 will shed more light on these questions.

B. Heisenberg-limit Scaling in Decision Quality

To analyze our results and compare to the traditional displacement sensing approaches, we plot the decision error of the QSPI protocol versus its degree d on a log-log plot as shown in Fig 7. This plot illuminates an interesting relationship between the QSPI protocol degree and the associated response function. From the figure, we can see that the numerical data points can be fitted by a linear black dashed line, demonstrating a power-law trend for p_{err} vs. degree d. The fitting reveals a slope of roughly $\alpha = -0.82 \pm 0.02$ which is close to the HL-like scaling as defined in Definition 1. This power-law fit does not precisely fit all of the points, and it exhibits a parity-dependence with respect to the probability of error. The slope is slightly worse than the exact Heisenberg-limit (green dotted line), while still clearly outperforming the standard quantum limit, a deficiency that is consistent with the additional logarithmic factor $\log(d)$, as explained in Eq. (36) of Sec. IV B. To make a more direct comparison, we also fit all data points for $d \geq 5$ using the analytical scaling in Eq. (36) (blue dashed
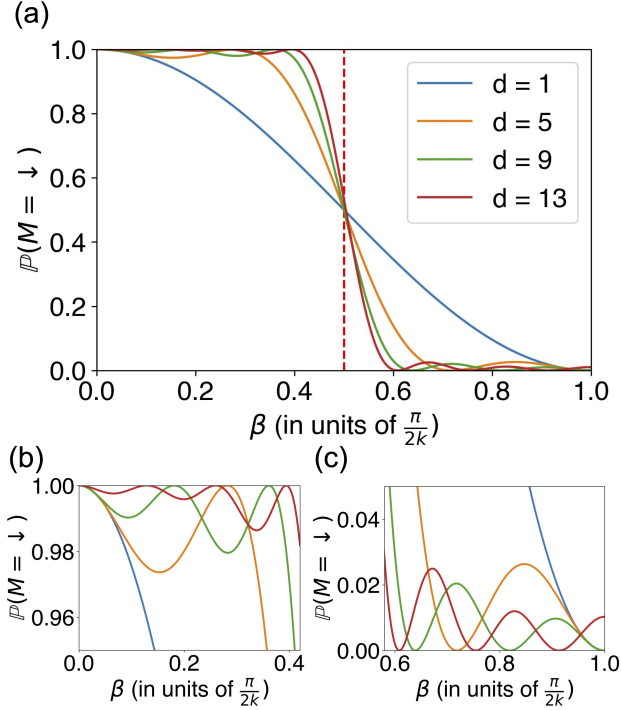
FIG. 6. (a) Example response functions for various degrees d for distinguishing a displacement with $\beta_{\text{th}} = 0.25 \cdot \frac{\pi}{\kappa}$, where $\kappa = 1/2048$, using QSPI phases from numerical optimization. (b, c) Magnified plots of the response function shown in (a) around $\mathbb{P}(M = \downarrow) = 0$ and $\mathbb{P}(M = \downarrow) = 1$, demonstrating that the response function for a d-QSPI protocol has $(d-1)$ turning points in the interval $[0, \frac{\pi}{2\kappa})$.
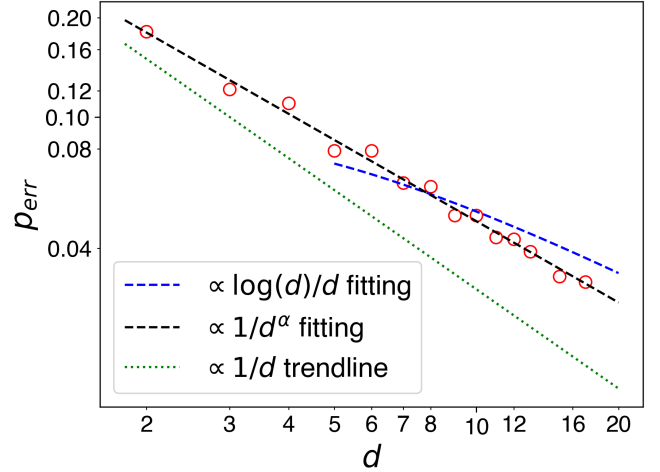

FIG. 7. Log-log scale plot of p_{err} versus the QSPI protocol degree d (red circles). The best-fit power-law scaling (black dashed line) has a slope of $\alpha = -0.82 \pm 0.02$, indicating $p_{\text{err}} \propto d^{-0.82\pm0.02}$. Best-fit theoretical scaling from Eq. (36) using data for $d \geq 5$ is shown with a blue dashed line. The $\propto 1/d$ HL scaling is shown with a green dotted line for comparison.

line). The difference between the analytical expectation and numerical data is because our analytical scaling is derived in the large d limit where we assume the major source of error p_{err} is from the falling edge as seen in Fig. 6 (also see discussion in Appendix D).

One final point is that although we were able to obtain numerical results and verify them, this brute-force optimization method does have several clear challenges. For example, to numerically optimize the sequence of phases minimizing the loss function (p_{err}), one must select an initial value for each of the phases as a starting point. It is possible that a sequence of initial values in the vicinity of a local minimum is selected and then the optimization procedure never escapes from the neighborhood around the local minimum. This problem becomes especially challenging for longer QSP sequences, where the search space is likely to contain more local minima. We attempt to address this difficulty by seeding with multiple distinct random initial phase sequences and iterating on only a subset with the least p_{err}. Thus, we

are able to increase the likelihood that we find a phase sequence that has not been trapped in a local minimum, allowing us to discern the optimal scaling of the decision error with QSPI degree.

C. Wigner Function of Optimal QSPI Sensing States

Given the numerically optimized phases for optimal QSPI sensing states, we may now visualize the resulting states to gain intuition about why their properties allow them to outperform cat states for our decision problems, as we describe in this section.

Although we learned the QSPI phases for the small $\kappa = 1/2048$ in order to best decouple the c_s coefficients and hence facilitate the optimization of the phases, bear in mind the discussion of the coupling of κ and β in Eq. (B8) and realize that we can adjust our choice of κ and the corresponding β with only minimal fine-tuning of the phases learned for the original value of κ. As such, for clearer visualization of low-degree states on the Wigner plots, we increase the scale of our problem by setting $\kappa = 0.15\sqrt{2}$ and setting $\beta_{\text{th}} = \frac{\pi}{4\kappa} = \frac{5\pi}{3\sqrt{2}}$. We use the phase sequence learned for $\kappa = \frac{1}{2048}$ as our initial phase sequence and resume optimization until convergence for the new value of κ. This change to κ results in minimal change to the QSPI phases during the optimization, with the majority of them differing by less than 1% relative to their original values. The Wigner plots for F and G (Eq. (9)) for the newly optimized states resulting from these d-QSPI protocols with $\kappa = 0.15\sqrt{2}$ are shown for $d = 5$, 9, and 13 in Subfigs. 8(d) – 8(i) in the lower half

of Fig. 8.

To compare these QSPI states with cat states, we plot F (Eq. (9a)) for cat states constructed with the same number $d-1$ of displacements by κ in Subfigs. 8(a) – 8(c) in the upper panel of Fig. 8. We see immediately that the interference patterns (regions with large contrast and Wigner negativity) for the cat state and QSPI state of same degree d differ significantly. The cat states display interference fringes from their two displaced coherent states that oscillate with a frequency of $\sqrt{2}d\kappa/\pi$ along the x-axis. Thus, cat states corresponding to higher degree d have higher-frequency fringes; this is what makes cat states effective sensors of very small displacements perpendicular to the coherent-state displacement in parameter-estimation protocols [15] but not optimal for making decisions about displacement. In fact, cat states have a constant probability of error p_{err} across all d for a given β_{th} and κ, as explained in Sec. IV A 1. In contrast, we have demonstrated both analytically and numerically that the QSPI sensing states can be designed to minimize the probability of error as the degree d is increased.

The physical intuition for this improved decision-making of the QSPI states stems from the lower-frequency features shown in the Wigner contrast plot. The spacing between sharp-Wigner-contrast features which appear consistently in the upper half of plots in Subfigs. 8(d) and 8(f) around $(x \approx \pm 1, p \approx 1)$ indicates the placement of sharp thresholds in the response function. This is why the cat-state response function places sharp thresholds with frequency $d\kappa/\pi$. In comparison, for general QSPI states, the interplay between asymmetric F and G is more complicated to analyze than for the F and G of cat states, but as we see in Fig. 8, the spacings between sharp Wigner features shown in Subfigs. 8(d) and 8(e) remain larger than those of the cat states shown in Subfigs. 8(a) and 8(b), respectively. Notice that the Wigner extent is also smaller for QSPI states as compared to cat state. This is because cat states are maximally extended in phase space for the given energy of the protocol by naively shifting the wave packet along one direction, while the QSPI state devotes some of the energy to creating a more complicated and optimized interference pattern phase space as compared to the simple sinusoid with Gaussian envelope that the cat state creates.

Subfigs. 8(g) – 8(i) then depict the final oscillator state after performing the entire QSPI displacement-sensing protocol with displacements by $\beta = \frac{1}{2}\beta_{\text{th}}$ and $\beta = \frac{3}{2}\beta_{\text{th}}$, conditioned on the qubit being in the $|\downarrow\rangle$ state. We note from these subfigures that the quasiprobability distribution exhibits primarily constructive interference to give a total $|\downarrow\rangle$-measurement probability of nearly 1 when the QSPI sensing protocol is applied for a displacement by $\beta = \frac{1}{2}\beta_{\text{th}}$, while the Wigner quasiprobability distribution exhibits primarily destructive interference to give a total $|\downarrow\rangle$-measurement probability of nearly 0 when the QSPI sensing protocol is applied for a displacement by $\beta = \frac{3}{2}\beta_{\text{th}}$ (hence the nearly

Sensing State	$\mathbb{P}(M = \downarrow \, | \beta = \frac{1}{2}\beta_{\text{th}})$	$\mathbb{P}(M = \downarrow \, | \beta = \frac{3}{2}\beta_{\text{th}})$
Cat State	0.957	0.035
QSPI 5	0.956	0.035
QSPI 9	0.976	0.021
QSPI 13	0.982	0.016

TABLE I. The probability of measuring the qubit in the $|\downarrow\rangle$ state after applying the entire sensing protocol with displacements by $\frac{1}{2}\beta_{\text{th}}$ (below threshold) and $\frac{3}{2}\beta_{\text{th}}$ (above threshold) using the cat state (independent of degree d) and the d-QSPI states for $d = 5$, 9, and 13, where $\kappa = 0.15\sqrt{2}$ and $\beta_{\text{th}} = \frac{\pi}{4\kappa} = \frac{5\pi}{3\sqrt{2}}$. These values are calculated from a numerical simulation of the QSPI protocol with a Fock-level truncation of $N = 500$ and using a grid with a grid spacing of 0.2×0.2. The numbers in the table are confirmed to converge to the significant figures with respect to both Fock-level truncation N and grid spacing by performing the same calculations with larger N and finer grids.

empty Wigner plots). These behaviors agree with our theoretical analysis and solve the Main Problem stated in Sec. II A.

In particular, we also show in Table I the probabilities of measuring $|\downarrow\rangle$ for the qubit state after performing the entire protocol with both the d-QSPI sensing states for $d = 5$, 9, and 13 and the corresponding cat states for reference. Note that according to simulation results (and as predicted in Sec. IV A 1), the probability of detection does not change with degree d for the cat state, so we provide only one probability. Note also from the results shown in the table that although the cat state performs well for sensing a displacement by β_{th} (with $\kappa = 0.15\sqrt{2}$ and $\beta_{\text{th}} = \frac{\pi}{4\kappa} = \frac{5\pi}{3\sqrt{2}}$), its performance is already matched with only a 5-QSPI state. Moreover, while the cat state's displacement-sensing performance remains constant with increasing degree d, the d-QSPI state's performance improves, so the 9- and 13-QSPI states outperform the cat state; moreover, performance of d-QSPI states for this displacement-sensing task will continue to improve as d increases further.

VII. CONCLUSION

In this paper, we present a general framework for single-shot quantum sensing using continuous-variable systems by establishing a theory of quantum signal processing interferometry. The basics of this construction are a generalization of QSP to systems with a qubit coupled to a quantum harmonic oscillator. The controlled displacement operation between the qubit and the oscillator forms a natural block-encoding of the displacement operator on the oscillators, via which arbitrary polynomial transformations on the oscillator's quadrature operator can be efficiently implemented. The flexibility of QSP provides the basis for our algorithmic QSPI sensing protocol. A measurement on the qubit induces a qubit response function that is a polynomial
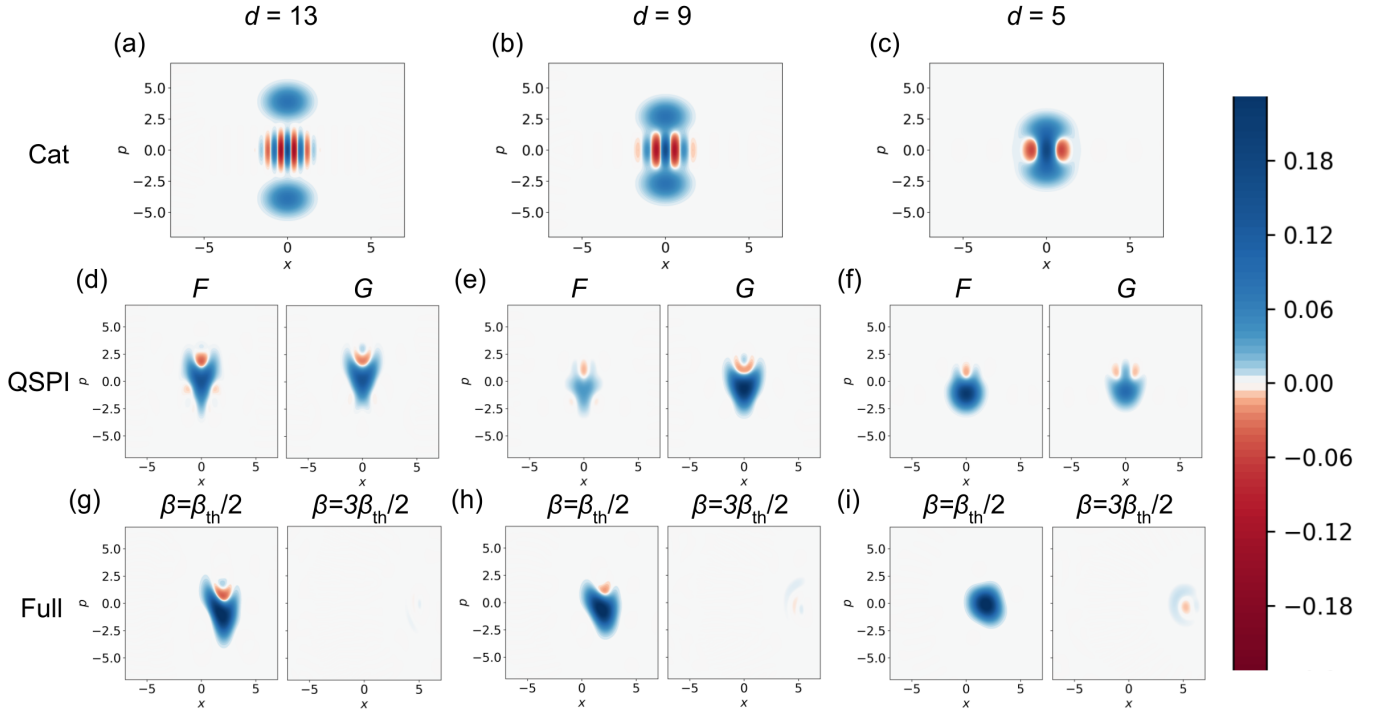
FIG. 8. Wigner plots of F for the cat state (Figs. 8(a), 8(b), and 8(c)), F and G for the optimal QSPI sensing state (Figs. 8(d), 8(e), and 8(f)), and the oscillator state resulting after the entire protocol is applied with displacements of $\beta = \frac{1}{2}\beta_{\text{th}}$ and $\beta = \frac{3}{2}\beta_{\text{th}}$ conditioned on the qubit being in the $|\downarrow\rangle$ state (Figs. 8(g), 8(h), and 8(i)) with $\kappa = 0.15\sqrt{2}$ and $\beta_{\text{th}} = \frac{\pi}{4\kappa} = \frac{5\pi}{3\sqrt{2}}$ constructed for $d = 13$, 9, and 5. Note the significant differences between the Wigner plots for the cat states and those for the QSPI sensing states, which do not closely resemble any known classes of quantum states. While the cat states all appear very similar but with more distance between their two coherent state parts and more interference fringes at the center as the degree d increases, the optimal sensing states have a more complex interference pattern for improved decision-making. As expected, the final oscillator state after the sensing protocol conditioned on the qubit being in the $|\downarrow\rangle$ state represents a probability close to 1 for a displacement by $\beta = \frac{1}{2}\beta_{\text{th}}$ but a small probability for a displacement by $\beta = \frac{3}{2}\beta_{\text{th}}$, matching the behavior of the calculated response functions, shown for $\kappa = \frac{1}{2048}$ in Fig. 6. A symmetrical logarithmic scale, where the scaling is logarithmic in both the positive and negative directions from a small linearly-scaling range around zero, is used as the color scheme in order to increase the contrast of finer features of the Wigner quasiprobability distribution.

transformation of the signal parameters that we would like to sense. By tuning the QSPI phase angles to design appropriate response functions, useful information about the signal parameters can be extracted efficiently.

The QSPI sensing protocol is analyzed in detail for a binary decision problem on a displacement channel with theoretical bounds on the sensing-circuit and sampling complexity. These binary decision oracles are then used to construct a composite protocol for parameter estimation via classical binary search and majority vote. Our sensing scheme is applied to determine if a displacement on the oscillator is greater or smaller than a certain threshold, and Heisenberg-limited behavior is derived analytically and observed numerically for this application.

While we have demonstrated Heisenberg-limited scaling for a binary decision on a displacement channel, the sensing protocol can be further improved. One immediate task is to determine if there exist non-optimization-based algorithms for finding QSPI phase angles that achieve a general QSPI response function.

This goal implies the need to find not only necessary but also sufficient conditions on QSPI for the backward direction of Theorem 4. Moreover, the sensing protocol for a single canonical variable of the oscillator can be generalized to two conjugate canonical variables of position and momentum simultaneously, allowing for the realization of quantum sensing in the entirety of phase space for the oscillator. Due to the Heisenberg uncertainty principle, tradeoffs between sensitivity in the position and momentum quadratures may be imposed using squeezing operations depending on the particular sensing task. In addition, the sensing power can be further enhanced by coherently manipulating multiple bosonic modes [20, 57], which can likely be coupled together with beamsplitters. In this context, tradeoffs between available quantum resources, such as space (number of oscillators) and time (sensing circuit depth), would be interesting to investigate.

The algorithmic QSPI-based quantum sensing protocol presented in this work opens many possibilities for useful applications. For example, bosonic modes appear in

many physical systems, such as in molecular vibrations and light-matter interactions under confined conditions. The displacement-sensing scheme presented here can be used to sense any chemical environment change in molecules, as long as the change leads to an effective displacement operation on molecular vibrations, as in the case of ro-vibrational coupling [58], or a displacement on photonic modes, as in polariton chemistry [59, 60]. The flexibility of designing response functions can also be used to deal with situations where the underlying signal has some prior distribution.

We note that the decomposition of composite sensing tasks, such as parameter estimation, into a series of decision problems provides ample room for the incorporation of hybrid quantum-classical algorithms into the sensing framework. For example, sophisticated adaptive strategies can be built in to gradually change the precision and shape of the decision filter and hence reduce the sensing cost. Lastly, Heisenberg-limited sensing is prone to quantum noise. It would be useful to analyze the stability of our QSPI-based continuous-variable sensing protocol in the presence of quantum noise [23, 61]. Realistic noise models on hardware containing bosonic degrees of freedom could be incorporated as well [62].

Appendix A: Proof of bosonic QSP Theorem 2

Denote the set of eigenvalues and eigenvectors of the generator $h(\hat{x},\hat{p})$ in Lemma 1 to be λ and $|\lambda\rangle$ such that

$$h(\hat{x},\hat{p})|\lambda\rangle = \lambda|\lambda\rangle. \qquad (A1)$$

Since $h(\hat{x},\hat{p})$ is Hermitian, we have $\lambda \in \mathbb{R}$. Moreover, for an infinite-dimensional oscillator, $\{\lambda\}$ can be inherently continuous. Furthermore, we assume that $\{|\lambda\rangle\}$ forms a (over)complete basis for the oscillator (for example, in the case of a continuous displacement operator whose eigenstates are coherent states) for achieving universal control of the oscillator. However, the bosonic QSP formalism still works in the subspace expanded by $\{|\lambda\rangle\}$.

Now, consider the action of W_z on an arbitrary qubit-oscillator entangled state, where the oscillator state

is given by $\frac{1}{\sqrt{2}}(|0\rangle|\Psi_0\rangle_{\mathrm{osc}} + |1\rangle|\Psi_1\rangle_{\mathrm{osc}})$. Expand the oscillator state under the $\{|\lambda\rangle\}$ basis to find

$$
\begin{aligned}
&W_z\frac{1}{\sqrt{2}}\left(|0\rangle|\Psi_0\rangle_{\mathrm{osc}} + |1\rangle|\Psi_1\rangle_{\mathrm{osc}}\right)\\
&=e^{-ih(\hat{x},\hat{p})\sigma_z}\frac{1}{\sqrt{2}}\left(|0\rangle|\Psi_0\rangle_{\mathrm{osc}} + |1\rangle|\Psi_1\rangle_{\mathrm{osc}}\right)\\
&=e^{-ih(\hat{x},\hat{p})\sigma_z}\frac{1}{\sqrt{2}}\left(|0\rangle\int d\lambda c_{0,\lambda}|\lambda\rangle + |1\rangle\int d\lambda c_{1,\lambda}|\lambda\rangle\right)\\
&=\frac{1}{\sqrt{2}}\left(|0\rangle\int d\lambda e^{-i\lambda}c_{0,\lambda}|\lambda\rangle + |1\rangle\int d\lambda e^{i\lambda}c_{1,\lambda}|\lambda\rangle\right)\\
&=\int d\lambda|\lambda\rangle\frac{1}{\sqrt{2}}\left(|0\rangle e^{-i\lambda}c_{0,\lambda} + |1\rangle e^{i\lambda}c_{1,\lambda}\right)\\
&=\int d\lambda|\lambda\rangle\otimes e^{-i\lambda\sigma_z}\left[\frac{c_{0,\lambda}|0\rangle + c_{1,\lambda}|1\rangle}{\sqrt{2}}\right]. \qquad (A2)
\end{aligned}
$$

Therefore, W_z acts individually on each 2×2 subspace labeled by the eigenvalue λ of $h(\hat{x},\hat{p})$ in a similar spirit to that of qubitization of a finite-dimensional block-encoding. From Eq. (A2), repeatedly applying W_z and a single-qubit rotation $e^{i\theta_j\sigma_x}$ will result in the application of QSP to each individual 2×2 subspace:

$$
\begin{aligned}
&e^{i\theta_d\sigma_x}\prod_{j=0}^{d-1}W_z e^{i\theta_j\sigma_x}\frac{1}{\sqrt{2}}(|0\rangle|\Psi_0\rangle_{\mathrm{osc}} + |1\rangle|\Psi_1\rangle_{\mathrm{osc}})\\
&=\int d\lambda|\lambda\rangle\otimes e^{i\theta_d\sigma_x}\prod_{j=0}^{d-1}e^{-i\lambda\sigma_z}e^{i\theta_j\sigma_x}\left[\frac{c_{0,\lambda}|0\rangle + c_{1,\lambda}|1\rangle}{\sqrt{2}}\right].
\end{aligned}
$$
$$(A3)$$

In the 2×2 subspace for each λ, the usual single-qubit QSP theorem applies and can achieve a Laurent polynomial transformation to the scalar $e^{-i\lambda}$. Performing the integral over all λ, it follows that the overall sequence in Eq. (8) performs a Laurent polynomial transformation on $e^{-ih(\hat{x},\hat{p})}$, hence proving Theorem 2.

Appendix B: Proof that the response function is a polynomial of the sensed signal

We prove in this section that the QSPI response function, as defined in Eq. (18), is a degree-d polynomial transformation of the new signal $v = e^{i(2\kappa)\beta}$ within a restricted range $[-\frac{\pi}{2\kappa}, \frac{\pi}{2\kappa}]$ and the polynomial is real.

Using the Laurent polynomial expressions in Eq. (9) and explicitly evaluating the integration with respect to x, we can write Eq. (18) as a series sum

$$\mathbb{P}(M =\downarrow|\beta) = \sum_{n,n',m,m'=-d}^{d} A_{n,n',m,m'}, \qquad (B1)$$

where

$$
\begin{aligned}
A_{n,n',m,m'} &= (f_n f_{n'} + g_n g_{n'})(f_m f_{m'} + g_m g_{m'})^*\\
&\quad \times e^{-\frac{1}{4}\kappa^2(n-n'-m+m')^2}e^{-i\kappa(n-m)\beta}. \qquad (B2)
\end{aligned}
$$

The following property can be verified:

$$A_{n,n',m,m'} = A^*_{m,m',n,n'}. \tag{B3}$$

$$\begin{aligned}
\mathbb{P}(M =\downarrow |\beta) &= \frac{1}{2} \sum_{n,n',m,m'=-d}^{d} (A_{n,n',m,m'} + A^*_{m,m',n,n'}) \\
&= \frac{1}{2}\left(\sum_{n,n',m,m'=-d}^{d} A_{n,n',m,m'} + \sum_{n,n',m,m'=-d}^{d} A^*_{m,m',n,n'} \right) \\
&= \frac{1}{2}\left(\sum_{n,n',m,m'=-d}^{d} A_{n,n',m,m'} + \sum_{n,n',m,m'=-d}^{d} A^*_{n,n',m,m'} \right) \\
&= \sum_{n,n',m,m'=-d}^{d} \mathrm{Re}\{A_{n,n',m,m'}\}, \tag{B4}
\end{aligned}$$

where we have renamed variables $m \leftrightarrow n$ and $m' \leftrightarrow n'$ from the second line to the third line, and $\mathrm{Re}\{\cdot\}$ denotes the real part.

Next, we prove that $\mathbb{P}(M =\downarrow |\beta)$ is a degree-d Laurent polynomial of $v = e^{i(2\kappa)\beta}$ in the range $[-\frac{\pi}{2\kappa}, \frac{\pi}{2\kappa}]$.

Because f_n, g_n are each coefficients of Laurent polynomials from QSP, it follows that $f_n, g_n \neq 0$ only for even n if d is even, or $f_n, g_n \neq 0$ only for odd n if d is odd. This means $A_{n,n',m,m'} \neq 0$ only when m, n have the same parity and m', n' have the same parity, which further suggests the variable substitution

$$m = n + 2s, \quad m' = n' + 2r, \tag{B5}$$

where $-d \leq s, r \leq d$. Substituting this back into Eq. (B2), we have

$$\begin{aligned}
A_{n,n',n+2s,n'+2r} &= (f_n f_{n'} + g_n g_{n'}) \\
&\quad (f_{n+2s} f_{n'+2r} + g_{n+2s} g_{n'+2r}) \\
&\quad e^{-\kappa^2(r-s)^2} e^{i(2\kappa)s\beta}. \tag{B6}
\end{aligned}$$

Further, substituting this back into Eq. (B1), we obtain

$$\begin{aligned}
&\mathbb{P}(M =\downarrow |\beta) \\
&= \sum_{n,n',s,r=-d}^{d} (f_n f_{n'} + g_n g_{n'})(f_{n+2s} f_{n'+2r} + g_{n+2s} g_{n'+2r}) \\
&\quad \times e^{-\kappa^2(r-s)^2} e^{i(2\kappa)s\beta} \\
&= \sum_{s=-d}^{d} c_s(\kappa) v^s, \tag{B7}
\end{aligned}$$

where $v = e^{i(2\kappa)\beta}$ and

$$\begin{aligned}
c_s(\kappa) &= \sum_{n,n',r=-d}^{d} (f_n f_{n'} + g_n g_{n'}) \\
&\quad (f_{n+2s} f_{n'+2r} + g_{n+2s} g_{n'+2r}) e^{-\kappa^2(r-s)^2}, \tag{B8}
\end{aligned}$$

with $f_n, g_n \in \mathbb{R}$, $c_s \in \mathbb{R}$.

Because the new signal operator v has an effective momentum of 2κ, this means that $\mathbb{P}(M =\downarrow |\beta)$ will be periodic with a reduced period of $[-\frac{\pi}{2\kappa}, \frac{\pi}{2\kappa}]$. It follows that the QSPI response function $\mathbb{P}(M =\downarrow |\beta)$ is a degree-d Laurent polynomial in the operator $v = e^{i(2\kappa)\beta}$.

Appendix C: Recursive relationship between the QSP coefficients

The probability of making the wrong decision can be efficiently computed classically from the original QSP phase angles. First, by using the following recursive relationship, all the QSP coefficients f_n, g_n can be computed. Second, the series sum in Eq. (28) can be evaluated explicitly using the computed f_n, g_n, without loss of numerical precision.

$$f_r^{(d+1)} = \begin{cases} \cos\phi_{d+1} f_{r-1}^{(d)}, & r = d, d+1 \\ -\sin\phi_{d+1} g_{r+1}^{(d)}, & r = -d, -d-1 \\ \cos\phi_{d+1} f_{r-1}^{(d)} - \sin\phi_{d+1} g_{r+1}^{(d)}, & |r| \leq (d-1) \end{cases} \tag{C1}$$

$$g_r^{(d+1)} = \begin{cases} \sin\phi_{d+1} f_{r-1}^{(d)}, & r = d, d+1 \\ \cos\phi_{d+1} g_{r+1}^{(d)}, & r = -d, -d-1 \\ \sin\phi_{d+1} f_{r-1}^{(d)} + \cos\phi_{d+1} g_{r+1}^{(d)}, & |r| \leq (d-1) \end{cases} \tag{C2}$$

Appendix D: Proof of Heisenberg scaling for QSPI binary decisions

From Fig. 4, the decision error probability can be approximately written as a sum of two contributions in the following way

$$p_{\text{err}} \approx \epsilon \left(\frac{\pi}{\kappa} - 2\sigma \right) + \frac{\sigma}{2},$$ (D1)

where ϵ is the approximation error to an ideal step function from a polynomial function. The first term in Eq. (D1) is obtained from such an imperfect polynomial approximation in the region of $[-\frac{\pi}{2\kappa}, \frac{\pi}{2\kappa}]$, excluding the rising and falling edges $[\beta_{\text{th}} - \sigma/2, \beta_{\text{th}} + \sigma/2] \cup [-\beta_{\text{th}} - \sigma/2, -\beta_{\text{th}} + \sigma/2]$; the second term in Eq. (D1) is from erroneous decisions when the displacement β lies within the rising or falling edge.

Rearranging Eq. (D1), this means that the error in the polynomial approximation to $P_{\text{ideal}}^{\text{sign,sin}}$ is

$$\epsilon \approx \frac{p_{\text{err}} - \frac{\sigma}{2}}{\frac{\pi}{\kappa} - 2\sigma}.$$ (D2)

From Ref. [36], to achieve an ϵ approximation to the sign function in regions excluding $[-\sigma/2, \sigma/2]$ requires a polynomial of degree $d = \gamma(\epsilon, \sigma)$ for

$$\gamma(\epsilon, \sigma) := 2 \cdot \left\lceil \max \left(\frac{e}{\sigma} \sqrt{W\left(\frac{8}{\pi\epsilon^2}\right) W\left(\frac{512}{e^2\pi}\frac{1}{\epsilon^2}\right)},\ \sqrt{2}W\left(\frac{8\sqrt{2}}{\sqrt{\pi}\sigma\epsilon}\sqrt{W\left(\frac{8}{\pi\epsilon^2}\right)}\right) \right) \right\rceil + 1,$$ (D3)

where $W(\cdot)$ is the Lambert W function. Assuming $\sigma = O(p_{\text{err}})$ and for small p_{err}, substitute Eq. (D2) into Eq. (D3) and use a Taylor expansion on the Lambert W function in order to obtain Eq. (35) in the main text.

[1] L. S. Collaboration and V. Collaboration, Phys. Rev. Lett. **116**, 061102 (2016).
[2] T. Bothwell, C. J. Kennedy, A. Aeppli, D. Kedar, J. M. Robinson, E. Oelker, A. Staron, and J. Ye, Nature **602**, 420 (2022).
[3] T. S. Roussy, L. Caldwell, T. Wright, W. B. Cairncross, Y. Shagam, K. B. Ng, N. Schlossberger, S. Y. Park, A. Wang, J. Ye, *et al.*, Science **381**, 46 (2023).
[4] V. Giovannetti, S. Lloyd, and L. Maccone, Science **306**, 1330 (2004), https://www.science.org/doi/pdf/10.1126/science.1104149.
[5] S. Boixo, A. Datta, M. J. Davis, S. T. Flammia, A. Shaji, and C. M. Caves, Phys. Rev. Lett. **101**, 040403 (2008).
[6] T. Tilma, S. Hamaji, W. J. Munro, and K. Nemoto, Phys. Rev. A **81**, 022108 (2010).
[7] D. Braun, G. Adesso, F. Benatti, R. Floreanini, U. Marzolino, M. W. Mitchell, and S. Pirandola, Rev. Mod. Phys. **90**, 035006 (2018).
[8] J. J. . Bollinger, W. M. Itano, D. J. Wineland, and D. J. Heinzen, Phys. Rev. A **54**, 4649 (1996).
[9] N. F. Ramsey, Physical Review (U.S.) Superseded in part by Phys. Rev. A, Phys. Rev. B: Solid State, Phys. Rev. C, and Phys. Rev. D **78**, 695 (1950).
[10] C. D. Marciniak, T. Feldker, I. Pogorelov, R. Kaubruegger, D. V. Vasilyev, R. van Bijnen, P. Schindler, P. Zoller, R. Blatt, and T. Monz, Nature **603**, 604 (2022), number: 7902 Publisher: Nature Publishing Group.
[11] R. Kaubruegger, D. V. Vasilyev, M. Schulte, K. Hammerer, and P. Zoller, Physical Review X **11**, 10.1103/physrevx.11.041045 (2021).
[12] E. Descamps, N. Fabre, A. Keller, and P. Milman, arXiv preprint arXiv:2210.05511 (2022).
[13] M. Penasa, S. Gerlich, T. Rybarczyk, V. Métillon, M. Brune, J. M. Raimond, S. Haroche, L. Davidovich, and I. Dotsenko, Phys. Rev. A **94**, 022313 (2016).
[14] K. Duivenvoorden, B. M. Terhal, and D. Weigand, Phys. Rev. A **95**, 012305 (2017).
[15] K. A. Gilmore, M. Affolter, R. J. Lewis-Swan, D. Barberena, E. Jordan, A. M. Rey, and J. J. Bollinger, Science **373**, 673 (2021).
[16] M. Tse, H. Yu, N. Kijbunchoo, A. Fernandez-Galiana, P. Dupej, L. Barsotti, C. D. Blair, D. D. Brown, S. E. Dwyer, A. Effler, M. Evans, P. Fritschel, V. V. Frolov, A. C. Green, G. L. Mansell, F. Matichard, N. Mavalvala, D. E. McClelland, L. McCuller, T. McRae, J. Miller, A. Mullavey, E. Oelker, I. Y. Phinney, D. Sigg, B. J. J. Slagmolen, T. Vo, R. L. Ward, C. Whittle, R. Abbott, C. Adams, R. X. Adhikari, A. Ananyeva, S. Appert, K. Arai, J. S. Areeda, Y. Asali, S. M. Aston, C. Austin, A. M. Baer, M. Ball, S. W. Ballmer, S. Banagiri, D. Barker, J. Bartlett, B. K. Berger, J. Betzwieser, D. Bhattacharjee, G. Billingsley, S. Biscans, R. M. Blair, N. Bode, P. Booker, R. Bork, A. Bramley, A. F. Brooks, A. Buikema, C. Cahillane, K. C. Cannon, X. Chen, A. A. Ciobanu, F. Clara, S. J. Cooper, K. R. Corley, S. T. Countryman, P. B. Covas, D. C. Coyne, L. E. H. Datrier, D. Davis, C. Di Fronzo, J. C. Driggers, T. Etzel, T. M. Evans, J. Feicht, P. Fulda, M. Fyffe, J. A. Giaime, K. D. Giardina, P. Godwin, E. Goetz, S. Gras, C. Gray, R. Gray, A. Gupta, E. K. Gustafson, R. Gustafson, J. Hanks, J. Hanson, T. Hardwick, R. K. Hasskew, M. C. Heintze, A. F. Helmling-Cornell, N. A. Holland, J. D. Jones, S. Kandhasamy, S. Karki, M. Kasprzack,

K. Kawabe, P. J. King, J. S. Kissel, R. Kumar, M. Landry, B. B. Lane, B. Lantz, M. Laxen, Y. K. Lecoeuche, J. Leviton, J. Liu, M. Lormand, A. P. Lundgren, R. Macas, M. MacInnis, D. M. Macleod, S. Márka, Z. Márka, D. V. Martynov, K. Mason, T. J. Massinger, R. McCarthy, S. McCormick, J. McIver, G. Mendell, K. Merfeld, E. L. Merilh, F. Meylahn, T. Mistry, R. Mittleman, G. Moreno, C. M. Mow-Lowry, S. Mozzon, T. J. N. Nelson, P. Nguyen, L. K. Nuttall, J. Oberling, R. J. Oram, B. O'Reilly, C. Osthelder, D. J. Ottaway, H. Overmier, J. R. Palamos, W. Parker, E. Payne, A. Pele, C. J. Perez, M. Pirello, H. Radkins, K. E. Ramirez, J. W. Richardson, K. Riles, N. A. Robertson, J. G. Rollins, C. L. Romel, J. H. Romie, M. P. Ross, K. Ryan, T. Sadecki, E. J. Sanchez, L. E. Sanchez, T. R. Saravanan, R. L. Savage, D. Schaetzl, R. Schnabel, R. M. S. Schofield, E. Schwartz, D. Sellers, T. J. Shaffer, J. R. Smith, S. Soni, B. Sorazu, A. P. Spencer, K. A. Strain, L. Sun, M. J. Szczepańczyk, M. Thomas, P. Thomas, K. A. Thorne, K. Toland, C. I. Torrie, G. Traylor, A. L. Urban, G. Vajente, G. Valdes, D. C. Vander-Hyde, P. J. Veitch, K. Venkateswara, G. Venugopalan, A. D. Viets, C. Vorvick, M. Wade, J. Warner, B. Weaver, R. Weiss, B. Willke, C. C. Wipf, L. Xiao, H. Yamamoto, M. J. Yap, H. Yu, L. Zhang, M. E. Zucker, and J. Zweizig, Phys. Rev. Lett. **123**, 231107 (2019).

[17] K. Gietka, Physical Review Research **4**, 043074 (2022).

[18] M. Kira, S. W. Koch, R. P. Smith, A. E. Hunter, and S. T. Cundiff, Nat. Phys. **7**, 799 (2011).

[19] Q. Zhuang, Z. Zhang, and J. H. Shapiro, Phys. Rev. A **97**, 032329 (2018).

[20] H. Kwon, Y. Lim, L. Jiang, H. Jeong, and C. Oh, Phys. Rev. Lett. **128**, 180503 (2022).

[21] H. Li, Y. Tong, H. Ni, T. Gefen, and L. Ying, Heisenberg-limited hamiltonian learning for interacting bosons (2023), arXiv:2307.04690 [quant-ph].

[22] H.-Y. Huang, Y. Tong, D. Fang, and Y. Su, Phys. Rev. Lett. **130**, 200403 (2023).

[23] Y. Dong, J. Gross, and M. Y. Niu, arXiv preprint arXiv:2209.11207 (2022).

[24] A. V. Oppenheim, *Discrete-time signal processing* (Pearson Education India, 1999).

[25] T. Parks and J. McClellan, IEEE Transactions on circuit theory **19**, 189 (1972).

[26] A. Antoniou, *Digital filters: analysis, design, and signal processing applications* (McGraw-Hill Education, 2018).

[27] G. H. Low, T. J. Yoder, and I. L. Chuang, Physical Review X **6**, 041067 (2016).

[28] G. H. Low and I. L. Chuang, Quantum **3**, 163 (2019).

[29] Y. Kikuchi, C. Mc Keever, L. Coopmans, M. Lubasch, and M. Benedetti, npj Quantum Information **9**, 93 (2023).

[30] Z. M. Rossi and I. L. Chuang, Quantum **6**, 811 (2022).

[31] Y. Dong, L. Lin, H. Ni, and J. Wang, arXiv preprint arXiv:2209.10162 (2022).

[32] Z. M. Rossi, V. M. Bastidas, W. J. Munro, and I. L. Chuang, arXiv preprint arXiv:2304.14383 (2023).

[33] D. Motlagh and N. Wiebe, arXiv preprint arXiv:2308.01501 (2023).

[34] L. Laneve, arXiv preprint arXiv:2311.03949 (2023).

[35] Z. M. Rossi, J. L. Ceroni, and I. L. Chuang, arXiv preprint arXiv:2309.16665 (2023).

[36] J. M. Martyn, Y. Liu, Z. E. Chin, and I. L. Chuang, The Journal of Chemical Physics **158** (2023).

[37] J. Wang, Y. Dong, and L. Lin, Quantum **6**, 850 (2022).

[38] J. M. Martyn, Z. M. Rossi, A. K. Tan, and I. L. Chuang, PRX Quantum **2**, 040203 (2021).

[39] Z. Yu, H. Yao, M. Li, and X. Wang, Advances in Neural Information Processing Systems **35**, 27810 (2022).

[40] P. C. Haljan, K.-A. Brickman, L. Deslauriers, P. J. Lee, and C. Monroe, Phys. Rev. Lett. **94**, 153602 (2005).

[41] A. Eickbusch, V. Sivak, A. Z. Ding, S. S. Elder, S. R. Jha, J. Venkatraman, B. Royer, S. M. Girvin, R. J. Schoelkopf, and M. H. Devoret, Nature Physics **18**, 1464 (2022).

[42] N. W. Ashcroft and N. D. Mermin, *Solid state physics* (Cengage Learning, 2022).

[43] S. Krastanov, V. V. Albert, C. Shen, C.-L. Zou, R. W. Heeres, B. Vlastakis, R. J. Schoelkopf, and L. Jiang, Phys. Rev. A **92**, 040303 (2015).

[44] B. Mischuck and K. Mølmer, Phys. Rev. A **87**, 022341 (2013).

[45] Y. Liu, J. Sinanan-Singh, M. T. Kearney, G. Mintzer, and I. L. Chuang, Phys. Rev. A **104**, 032605 (2021).

[46] A. M. Childs and N. Wiebe, Quantum Information & Computation **12**, 901 (2012).

[47] D. W. Berry, A. M. Childs, R. Cleve, R. Kothari, and R. D. Somma, Physical Review Letters **114** (2015).

[48] J. Haah, Quantum **3**, 190 (2019), arXiv:1806.10236 [quant-ph].

[49] A. Blais, R.-S. Huang, A. Wallraff, S. M. Girvin, and R. J. Schoelkopf, Phys. Rev. A **69**, 062320 (2004).

[50] C. Monroe, D. M. Meekhof, B. E. King, and D. J. Wineland, Science **272**, 1131 (1996).

[51] C. W. Helstrom, Journal of Statistical Physics **1**, 231 (1969).

[52] J. S. Geronimo and H. J. Woerdeman, Annals of Mathematics , 839 (2004).

[53] R. Chao, D. Ding, A. Gilyen, C. Huang, and M. Szegedy, Finding Angles for Quantum Signal Processing with Machine Precision (2020), arXiv:2003.02831 [quant-ph].

[54] Quantum Signal Processing Interferometry, https://github.com/yuanliu1/QSP-Interferometry (2023).

[55] A. V. Oppenheim, *Discrete-time signal processing*, 3rd ed., Prentice Hall signal processing series (Pearson, Upper Saddle River [N.J, 2010).

[56] Y. C. Kuyu and F. Vatansever, AEU-International Journal of Electronics and Communications **70**, 1651 (2016).

[57] Q. Zhuang, Z. Zhang, and J. H. Shapiro, Phys. Rev. A **97**, 032329 (2018).

[58] C. L. Pekeris, Phys. Rev. **45**, 98 (1934).

[59] R. F. Ribeiro, L. A. Martínez-Martínez, M. Du, J. Campos-Gonzalez-Angulo, and J. Yuen-Zhou, Chemical science **9**, 6325 (2018).

[60] W. Xiong, Accounts of Chemical Research **56**, 776 (2023).

[61] H. Xu, B. Wang, H. Yuan, and X. Wang, arXiv preprint arXiv:2309.05592 (2023).

[62] A. J. Brady, A. Eickbusch, S. Singh, J. Wu, and Q. Zhuang, arXiv preprint arXiv:2308.02913 (2023).